Journal Pre-proof

A comparative study of hyperelastic constitutive models for colonic tissue fitted to multiaxial experimental testing

S. Puértolas, E. Peña, A. Herrera, E. Ibarz, L. Gracia

PII: S1751-6161(19)31041-0

DOI: https://doi.org/10.1016/j.jmbbm.2019.103507

Reference: JMBBM 103507

To appear in: *Journal of the Mechanical Behavior of Biomedical Materials*

Received Date: 24 July 2019

Revised Date: 4 October 2019

Accepted Date: 23 October 2019

Please cite this article as: Puértolas, S., Peña, E., Herrera, A., Ibarz, E., Gracia, L., A comparative study of hyperelastic constitutive models for colonic tissue fitted to multiaxial experimental testing, *Journal of the Mechanical Behavior of Biomedical Materials* (2019), doi: https://doi.org/10.1016/j.jmbbm.2019.103507.

Colonic tissue

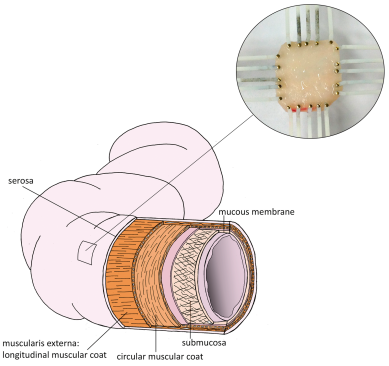

Experimental tests

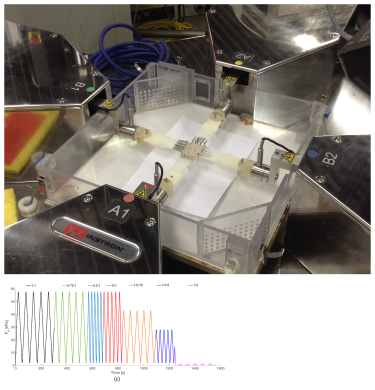

Mechanical characterization

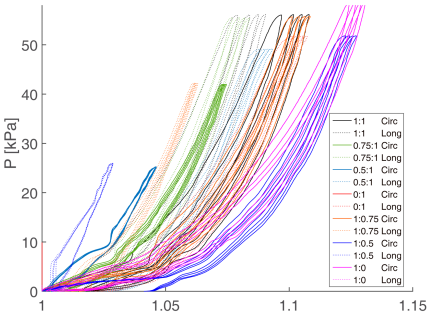

A comparative study of hyperelastic constitutive models for colonic tissue fitted to multiaxial experimental testing

S. Puértolas[a,b*], E. Peña [a,b,e], A. Herrera[b,c,d], E. Ibarz[a,b], L. Gracia[a,b]

[a] Department of Mechanical Engineering, University of Zaragoza. Zaragoza, Spain

[b] Aragón Institute for Engineering Research. Zaragoza, Spain

[c] Department of Surgery, University of Zaragoza. Zaragoza, Spain

[d] Aragón Health Research Institute. Zaragoza, Spain

[e] CIBER de Bioingeniería, Biomateriales y Nanomedicina. CIBER-BBN. Zaragoza, Spain

[*] Corresponding author:

E-mail: spb@unizar.es

Address: Department of Mechanical Engineering.

EINA – Engineering and Architecture School

University of Zaragoza

María de Luna, s/n (Edif. Betancourt)

50018 – Zaragoza (SPAIN)

Email addresses:

EP : fany@unizar.es Estefanía Peña

AH : antonio.herrera@unizar.es Antonio Herrera

EI : eibarz@unizar.es Elena Ibarz

LG : lugravi@unizar.es Luis Gracia

Abstract

For colonic stents design, the interaction with colonic tissue is essential in order to characterize the appropriate radial stiffness which provides a minimum lumen for intestinal transit to be maintained. It is therefore important to develop suitable constitutive models allowing the mechanical behavior of the colon tissue to be characterized.

The present work investigates the biomechanical behavior of colonic tissue by means of biaxial tests carried out on different parts of the colonic tract taken from several porcine specimens. Samples from the colonic tract were quasi-statically tensioned using a load-controlled protocol with different tension ratios between the circumferential and the axial directions. Fitting techniques were then used to adjust specific hyperelastic models accounting for the multilayered conformation of the colonic wall and the fiber-reinforced configuration of the corresponding tissues.

It was found that the porcine colon changed from a more isotropic to a more anisotropic tissue and became progressively more flexible and compliant in circumferential direction depending on the position along the duct as it approaches the rectum. The best predictive capability of mechanical behavior corresponds to the Four Fiber Family (FFF) model showing mean values of coefficient of determination $R^2 = 0.97$, and a normalized root mean square error of $\varepsilon_{NRMS} = 0.0814$ for proximal spiral samples, and $R^2 = 0.89$, $\varepsilon_{NRMS} = 0.1600$ and $R^2 = 0.94$, $\varepsilon_{NRMS} = 0.1227$ for distal spiral and descending colon samples, respectively. The other analyzed models provide good results for proximal spiral colon specimens, which have a lower degree of anisotropy.

The analyzed models with the fitted elastic parameters can be used for more realistic and reliable FE simulations, providing the appropriate framework for the design of optimal devices for the treatment of colonic diseases.

Key words

Biaxial experimental testing

Descending colon

Colonic tissue biomechanics

Hyperelastic constitutive models

1. Introduction

Many pathologies of the digestive system occur in the colon. Diseases such as diverticulosis, inflammatory bowel syndrome and cancer are the most common [1, 2]. A high percentage of them cause varying degrees of obstruction in the colon, which is treated using self-expanding stents. Unfortunately, no long-term minimally invasive solutions are currently available for treatment of these pathologies.

To reproduce realistic biomechanical behavior in computational simulations of digestive surgery procedures and to design safe and effective therapeutic devices (i.e., rectal catheters and colonic stents), it is important to develop suitable constitutive models allowing the mechanical behavior (stress-strain relation) of the colon tissue to be characterized. Such models would enable a more accurate analysis of the propulsion of stools along the colon during digestion, of the risk of perforation during occlusions, and of the interaction phenomena between biological tissues and biomedical devices.

Traditionally, porcine tissue has been used for the modeling of various human tissues in medicine due to their size, physiological and functional similarities, as well as the ease of procurement. In the scientific literature, it is usually accepted that human and pig colon morphology and dimensions appear similar [3]. However, the human colon is shorter (measuring up to about 1.5 meters as against 4.5 meters in pigs) and has five main regions: Cecum, ascending colon, transverse colon, descending colon, and sigmoid colon. The pig colon has three regions: Cecum, spiral colon (proximal), and descending colon (distal). Despite these differences, the potential similarities and the existence of available biomechanical data make porcine tissue a potentially ideal model for obtaining valuable information for characterizing the biomechanical behavior of colorectal tissue.

It is well known that the reliability of biomechanical simulation models depends on the appropriate material behavior characterization, especially in the case of soft tissues. For colonic stents design, the interaction with colonic tissue is essential in order to characterize the appropriate radial stiffness which allows a suitable lumen for intestinal transit to be maintained [4, 5].

There are not many publications in the specialized literature that provide experimental test data relating to colonic tissues, and even fewer studies of constitutive models that reproduce the tissue behavior in order to obtain more reliable results in numerical simulations.

Among the published works, a few reports can be found of tensile tests performed on human colon tissue. Ergov et al. (2002) [6] and more recently Massalou et al. (2016) [7] present different results corresponding to uniaxial dynamic tensile tests. However, there are several reports of biomechanical characterization of colon tissue from common laboratory animals using different mechanical tests and constitutive models: tests of compression in goat colon [8], tensile tests and a constitutive model for pig colon tissue [9-11], extension-inflation tests and a constitutive model for pig colon tissue [12] and tensile tests and biomechanical characterization of rat colon [13, 14]. Finally, in Carniel et al. (2014) [15] a physio-mechanical model by means of an inflation test is proposed. Uniaxial tensile tests do not provide enough information in order to appropriately characterize the mechanical behavior of colonic tissue. More complex tests are recommended, as for example biaxial tests [16, 17] or inflation tests, because they subject the sample to a stress state closer to the actual physiological conditions.

To the best of our knowledge, there are no works concerning biaxial testing of porcine colonic tissue in the specialized literature. A biaxial test study has recently been published but this refers to mouse colorectal specimens [18]. The present study concerning biaxial tests for samples obtained from different locations of the porcine colon may therefore be considered a highly original contribution.

Despite the above-mentioned works, there is no general consensus about the most appropriate model for colorectal tissue modeling in numerical simulations, due to the inherent complexity involved. In this context, the objective of the present work is to investigate the biomechanical behavior of colonic tissue by means of biaxial tests carried out in different parts of the colonic tract taken from several porcine specimens, taking into account the morphologic similarities with the human colon. Fitting

techniques are then used to adjust specific hyperelastic models accounting for the multilayered conformation of the colonic wall and the fiber-reinforced configuration of the corresponding tissues.

2. Materials and Methods

2.1. Colon physiology

The colon has an almost cylindrical shape with a lumen of variable diameter surrounded by a wall composed of four main layers (from the lumen outwards): the mucosa, submucosa, muscularis externa, and serosa. The mucosa membrane, the inner lining of the colonic tract, is made up of epithelial lining, a lamina propria of loose connective tissue and a muscularis mucosa. The submucosa is a layer of dense irregular connective tissue with large blood vessels and lymphatic vessels. Its main mechanical components are collagen fibers arranged in a criss-cross pattern [19, 20]. The muscularis externa is composed of two muscular layers, an internal layer whose fibers are arranged in a circumferential direction, and an external layer with fibers in a longitudinal direction (Fig. 1). Both are responsible for segmentation and peristalsis motions (the mechanical processing and movement of materials along the digestive tract). The Serosa is a layer of squamous epithelium covering the muscularis externa with a dense sheath of collagen fibers that firmly attaches the colonic tract to adjacent structures called the adventitia.

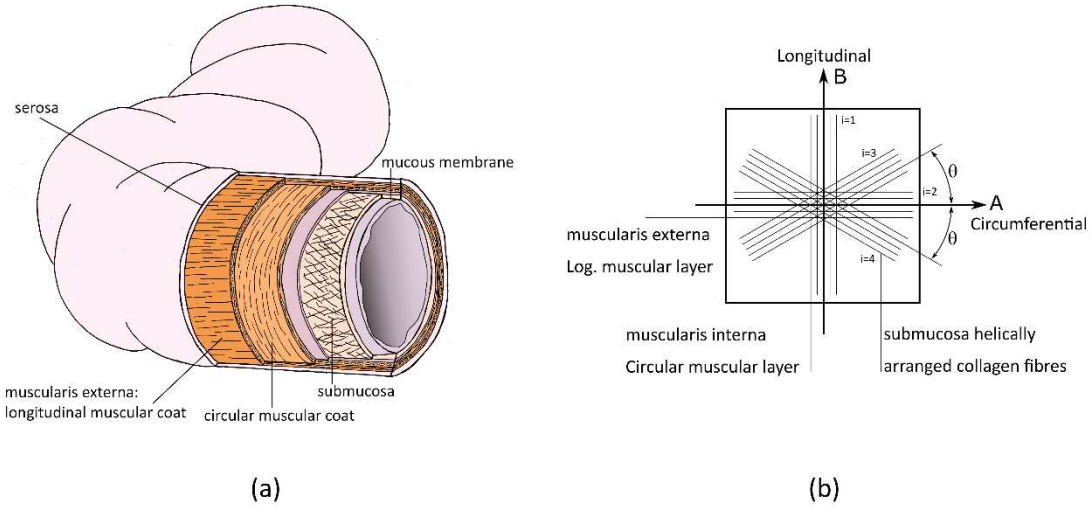

Fig. 1. Schematic representation of physiological structure of the colon: (a) configuration by layers of the colonic duct; (b) schematic diagram of collagen fibers arrangement and their correlation with the different layers.

Thus, colonic tissue is a composite biological structure producing a complex mechanical response involving non-linear, anisotropic and time-dependence behavior. As explained above, the colon is composed of several tissue layers. Within each layer, different fiber families are distributed according to specific spatial orientations, which lead to a strongly anisotropic configuration.

2.2. Experimental tests

The experimental tests were performed on tissue specimens taken from pig colon, given the similarity between pig and human tissue mechanics reported in some studies. The sacculated shape of the spiral colon due to the taeniae is very similar to that observed in humans, and the wall of the descending colon appears smooth due to less pronounced taeniae in that region. The most usual colonic stent insertion sites are in the zone of the descending and sigmoid colon. Therefore, the present study is focused on the analogous parts of the porcine large intestine. Due to the great length of the spiral colon, it is divided into two zones to detect possible behavior variations along the duct. These are defined as the proximal and distal spiral, followed by descending colon.

The whole large intestine of five female porcine subjects (aged 5–6 months and a weight of 95-105 kg) were sectioned and removed postmortem. Immediately, the luminal content was drained and carefully flushed with a 0.9% NaCl physiological saline solution (PSS). Porcine bowel tissues were kept frozen at − 80°C until testing. Once defrosted, samples were preserved in ion-free PSS (0.9% NaCl) at 4° C until preparation for mechanical testing. Specimens from the spiral colon (both proximal and distal) and descending colon were tested to investigate the potential regional variability of the mechanical behavior. A total of 56 biaxial tests were performed at different locations of the large intestine: 18 in the proximal spiral colon area (PS), 25 in the distal spiral colon area (DS), and 13 in the descending colon area (DC). Some problems appeared during testing (sliding at fixations, tissue tear, premature rupture) and many samples were discarded. Finally, 4/5 valid samples for each of the studied areas were selected for processing.

Tests were carried out in a high precision drive system adapted for biological specimens, an Instron BioPuls™ low-force planar-biaxial testing system (Fig. 2a), immersed in a bath filled with PSS and maintained at 37 °C by a circulation heater. Square specimens were mounted in the planar-biaxial machine by connecting five arms to each gag axis with clamp needles. The gag arms mechanism allows free displacements at the perpendicular direction to the arm. Needles attaching the specimen were located as close as possible to the edges to minimize the edge effects on strain measurements (Fig. 2b).

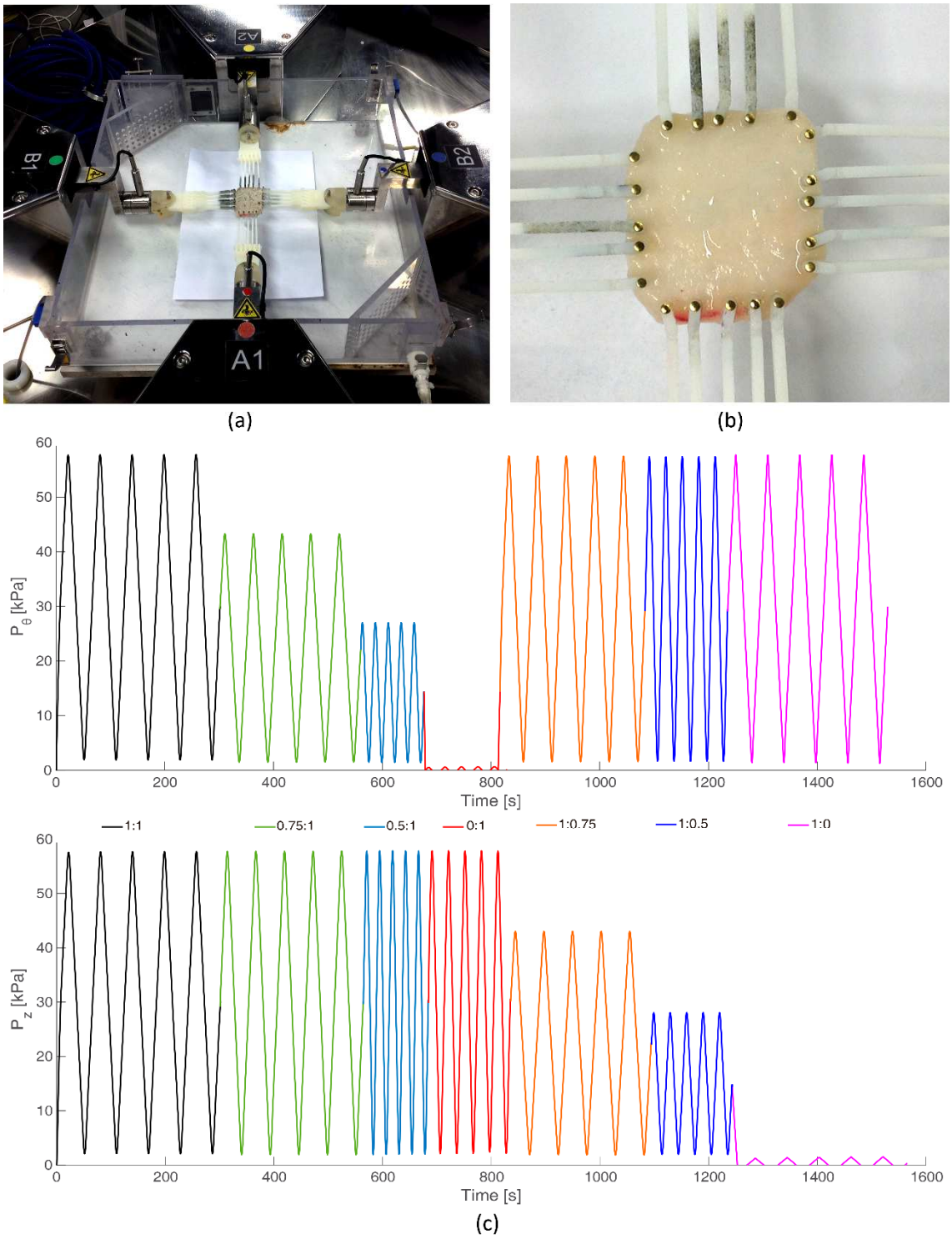

Fig. 2. Testing mounting, instrumentation and protocol: (a) Instron BioPuls™ biaxial tensile testing device; (b) specimen fixations system; (c) Testing loading history. Representation of biaxial tests protocol performed on experimental samples. Evolution of the 1st Piola-Kirchhoff (engineering) stress for each axis (P_θ: P_z).

For the biaxial tensile tests, square specimens of approximately 30x30 mm were cut from the spiral colon in the proximal and distal zones and from the descending colon using a punch cutter and a scalpel. The specimens were prepared with their sides

aligned in the circumferential and axial directions of the colonic duct (Fig. 1b). A caliper gauge and a Mitutoyo Digimatic micrometer were used to measure the length, width and thickness of the samples, and taking the mean value of 3 measures of them.

The samples were quasi-statically tensioned using a load-controlled protocol with different tension ratios between the circumferential and the axial direction (P_θ:P_z) corresponding to values of 1:1, 0.75:1, 0.5:1, 0:1, 1:0.75, 1:0.5, 1:0, respectively (Fig. 2c). Tests were carried out at stress rates of approximately 2kPa/s [21]. A maximum engineering stress (First Piola Kirchhoff stress tensor **P**) of 60 kPa was reached in every cyclic test (i.e. 1:1 corresponds to 60:60 KPa).

The test protocol considers 5 loading cycles for each stress ratio: every specimen was preconditioned through five loading–unloading cycles (Figs. 3a, 5a and 7a), and the last cycle (fifth, Figs. 3b, 5b and 7b) was used for further analysis [22]. A randomized points cloud of black markers was attached on the surface of the specimen for deformation measurements with the video-extensometer [23, 24] using a Digital Image Correlation (DIC) Strain Master LaVision System equipped with two high performance digital cameras with a megapixel sensor (2.5 [µm] ± 0.5%).

2.3. Constitutive models

The mechanical response of colonic tissue subject to loading, like many other soft biological tissues, exhibits strong nonlinearity, large strains and anisotropic elastic behavior due to the presence of preferred directions in its microstructure and reorientation of the fiber directions with deformation. The simulation of these nonlinear effects requires constitutive models formulated within the framework of anisotropic hyperelasticity by defining strain energy functions (SEF).

In order to select the most suitable constitutive model (to reproduce and predict the mechanical response of the colon) which could be used in computational simulations, five SEFs were considered.

2.3.1. Holzapfel-Gasser-Ogden (HGO) model

This model corresponds to a hyperelastic anisotropic behavior proposed by Holzapfel et al. [25] for stress-strain description. The model is characterized by an isotropic

matrix of neo-Hookean form and the anisotropic contribution of two collagen fiber layers reinforcing the colon wall.

The model assumes that both families of fibers are symmetrical and mechanically equivalent (they have the same mechanical response). The anisotropy directions adopted describe a helical shape oriented at ±θ degrees relative to the circumferential direction. This model uses an exponential function for describing the SEF in the collagen fibers:

$$\Psi = \mu(I_1 - 3) + \sum_{i=4,6} \left\{ \frac{k_1}{2k_2} e^{k_2(I_i-1)^2} - 1 \right\} \quad (1)$$

where I_1 is the first invariant of the right Cauchy-Green deformation tensor $\mathbf{C}$ ($I_1 = tr\,\mathbf{C} = \lambda_\theta^2 + \lambda_z^2$). The anisotropic invariants: $I_4 = \mathbf{C} : \mathbf{M_{01}}$ and $I_6 = \mathbf{C} : \mathbf{M_{02}}$ are related to two families of fibers in each layer, where $\mathbf{M}_{0i} = \mathbf{m}_{0i} \otimes \mathbf{m}_{0i}$ are structural tensors referring to an individual family of fibers. Using the direction vectors $\mathbf{m}_{01} = (\cos\theta,\ \sin\theta,\ 0)^T$ and $\mathbf{m}_{02} = (\cos\theta, -\sin\theta,\ 0)^T$ specifying the orientation of the fibers, where θ represents the angle between each fiber family with respect to the circumferential direction in the undeformed configuration. So, the anisotropic invariants are:

$$I_4 = \lambda_\theta^2 \cos^2(\theta) + \lambda_z^2 \sin^2(\theta) \quad (2)$$

$$I_6 = \lambda_\theta^2 \cos^2(-\theta) + \lambda_z^2 \sin^2(-\theta) \quad (3)$$

Finally, μ >0 is a stress-like material constant describing the isotropic matrix response, $k_1 > 0$ is a stress-like constant defining the layer stiffness of collagen fibers, and $k_2 > 0$ is a dimensionless material parameter related to the progressivity of fiber stiffening behavior during deformation.

It is assumed that the strain energy corresponding to the anisotropic terms only contributes to the global mechanical response of the tissue when stretched (invariants

$I_4 > 1$ and $I_6 > 1$). Therefore, a total of 4 elastic parameters ($\mu,\ k_1,\ k_2, \theta$) should be fitted to define the stress-strain behavior.

2.3.2. Gasser-Ogden-Holzapfel (GOH) model

This model proposed by Gasser et al. [26] is based on the previous HGO model [25] introducing generalized structural tensors of an individual family of fibers $\boldsymbol{H_i}=\kappa \cdot \mathbf{1} + (1-3\kappa)\mathbf{M}_{0i}$; where $\mathbf{1}$ is the identity tensor and $\mathbf{M}_{0i} = \mathbf{m}_{0i} \otimes \mathbf{m}_{0i}$ is a structural tensor defined using unit vectors $\mathbf{m}_{01} = (\cos\theta,\ \sin\theta,\ 0\ )^T$, and $\mathbf{m}_{02} = (\cos\theta, -\sin\theta,\ 0\ )^T$ specifying the mean orientation of fibers. The SEF is defined as:

$$\Psi = \mu(I_1 - 3) + \sum_{i=4,6} \left\{ \frac{k_1}{2k_2} e^{k_2(\widehat{E}_i)^2} - 1 \right\} \tag{4}$$

where the parameter $\widehat{E}_i=\kappa I_1 + (1-3\kappa)I_i - 1\ ;\ i = 4, 6$ is introduced, representing the average strain measure of fibers for the layer i , and $\kappa\ \in [0,\ 1/3]$ is a parameter describing the dispersion of each fiber family orientation around its θ direction and is defined through $\kappa = \frac{1}{4}\int_0^\pi \rho \sin^3\theta\ d\theta$; $\kappa = 0$ describes the total alignment of all collagen fibers in θ direction, and $\kappa = 1/3$ corresponds to the maximum dispersion with random/isotropic fiber distribution [27]. This constitutive model therefore requires a total of 5 elastic parameters $(\mu, k_1, k_2, \kappa, \theta)$ that should be fitted.

2.3.3. Four-Fiber-Family model (FFF)

The third constitutive model, called Four Fiber Family (FFF), is a hyperelastic anisotropic model proposed by Baek et al. [28] and Ferruzzi et al. [29] for the stress-strain description of aortas and aneurysms. It is a variation of the HGO model, in which two more fiber families are added in longitudinal and circumferential orientations respectively. This model therefore presents a total of four families of fibers; one axial, one circumferential and two symmetrical in diagonal directions. Its SEF adopts the following expression:

$$\Psi = \mu(I_1 - 3) + \sum_{i=1,4} \left\{ \frac{k_{1i}}{2k_{2i}} e^{k_{2i}(I_{4i}-1)^2} - 1 \right\} \quad (5)$$

where I_1 is the first invariant of the right Cauchy-Green deformation tensor $\mathbf{C}$, and the invariants $I_{4i} = \mathbf{C} : \mathbf{M_{0i}}$ are related to four families of fibers; $\mathbf{M}_{0i} = \mathbf{m}_{0i} \otimes \mathbf{m}_{0i}$ are structural tensors referring to the four individual families of fibers ($i = 1$ to 4), and $\mathbf{m}_{0i}$ are unit vectors defining the orientation of individual fiber families (Fig.1b.); $i = 1$ corresponds to axis 2 (axial) $\mathbf{m}_{01} = (0, 1, 0)^T$, $i = 2$ corresponds to axis 1 (circumferential) $\mathbf{m}_{02} = (1, 0, 0)^T$, $i = 3$ (diagonal direction $+\theta$) $\mathbf{m}_{03} = (\cos\theta, \sin\theta, 0)^T$, and $i = 4$ (diagonal direction $-\theta$) $\mathbf{m}_{04} = (\cos\theta, -\sin\theta, 0)^T$. So: $I_{41} = \lambda_z^2$, $I_{42} = \lambda_\theta^2$, $I_{43} = \lambda_\theta^2 \cos^2(\theta) + \lambda_z^2 \sin^2(\theta)$, and $I_{44} = \lambda_\theta^2 \cos^2(-\theta) + \lambda_z^2 \sin^2(-\theta)$.

Finally, μ >0 is a stress-like material constant describing the isotropic matrix response, $k_{1i} > 0$ is a stress-like constant defining the stiffness of each layer of the collagen fibers, and $k_{2i} > 0$ represents dimensionless parameters referring to collagen-based stiffening during deformation. It is assumed that diagonal family fibers with an orientation angle θ (measured from axis 1 circumferential) are mechanically equivalent [29], thus $k_{13} = k_{14}$ and $k_{23} = k_{24}$. Thus, a total of 8 material parameters ($\mu, k_{11}, k_{21}, k_{21}, k_{22,}\ k_{13}, k_{23}, \theta$) should be fitted.

2.3.4. Microstructural models (MFM and MFB)

Finally, the last constitutive models correspond to microstructural models initially proposed by Lanir [30], assuming the total response of fibers as a sum of responses from all the fibers (in all directions) distributed in the three-dimensional (3D) Euclidean space. The distribution of fibers is described by an appropriate probabilistic distribution function also called orientation density function (ODF), so that the directional arrangement of fibers and directional dependence of other material parameters can be taken into account. The model is characterized by an isotropic matrix (analogous to the models described above) and by reinforcing collagen fibers with orientation defined through the appropriate ODF [31, 32].

The microfiber model takes into account the dispersion of the collagen fibers around a preferential direction, overcoming the 1D limitation of previous characterizations of the collagen fiber [33]. The SEF function is defined by the addition of two terms, corresponding to the contribution of the ground isotropic matrix and collagen fibers. It is written as:

$$\Psi = \mu(I_1 - 3) + \Psi_f \tag{6}$$

where Ψ_f refers to the collagen fiber contribution, and is defined as the sum of the contributions of each collagen family of fibrils, so that:

$$\Psi_f = \sum_{j=1}^{N} [\Psi_f]_j = \sum_{j=1}^{N} \langle n\rho\psi_f \rangle_j = \sum_{j=1}^{N} \frac{1}{4\pi} \int_{\mathbb{U}^2} \left(n\rho[\psi_f]\right)_j dA \tag{7}$$

where the average of the n contributions is denoted by the notation $\langle\cdot\rangle$, N corresponds to the number of families of collagen fibers, according to experimental results, N=2. The integration of the fiber stress over a unit sphere $\mathbb{U}^2$ can be written in a discretized way as:

$$[\Psi_f]_j = \sum_{i=1}^{m} w_i n\rho\left(\boldsymbol{r}_i; \lambda_{f\,i}\right) \psi_{f\,i} \tag{8}$$

which represents the contribution of the fibers, where $\boldsymbol{r}_i$ expresses the unit vectors associated with the discretization on the micro-sphere, m is the number of discrete orientation vectors [34], $\lambda_{f\,i} = \|\boldsymbol{F} \cdot \boldsymbol{r}_i\|$ the stretch in the $\boldsymbol{r}_i$ direction and $\psi_{f\,i}(\lambda_{f\,i})$ the strain energy function associated to the corresponding $\boldsymbol{r}_i$ direction. Including Eq. (8) in Eq. (7) one can get:

$$\Psi_f = \sum_{j=1}^{N} \sum_{i=1}^{m} \left(w_i n\rho[\psi_{f\,i}]\right)_j \tag{9}$$

where w_i denotes related weighting factors associated with the integration, and ρ is the orientation density function (ODF) to take into account the fiber dispersion [34].

An exponential strain energy function like that proposed in Holzapfel et al. (2000) [25] was used to model the fiber response

$$\psi_{f\,i}(\lambda_{f\,i}) = \begin{cases} 0 & if \quad \lambda_{f\,i} < 1 \\ \frac{c_1}{2c_2}\left[\exp\left(c_2\left[{\lambda_{f\,i}}^2 - 1\right]^2\right) - 1\right] & if \quad \lambda_{f\,i} \geq 1 \end{cases} \tag{10}$$

where c_1 is a stress-valued constant, c_2 is a dimensionless parameter, and $\lambda_{f\,i}$ the stretch in the fiber direction of $\boldsymbol{r}_i$.

To evaluate the fiber distribution, two different approaches have been adopted to define the ODF, which are known as Microfiber von Mises model (MFM) and Microfiber Bingham Model (MFB).

2.3.4.1 Microfiber Von Mises Model (MFM)

In this case, a bi-π-periodic von Mises ODF is adopted for the incorporation of anisotropy in the microsphere-based model previously described [34]. So, the orientation density function ρ is expressed as the sum of two transversely isotropic and π-periodic von Mises functions ρ_i and takes the form:

$$\rho(\theta) = \rho_1(\theta) + \rho_2(\theta) \tag{11}$$

with

$$\rho_i(\theta) = 4\sqrt{\frac{b}{2\pi}}\frac{\exp(b[\cos(2\theta) + 1])}{\operatorname{erfi}(\sqrt{2b})} \tag{12}$$

where $\theta = \arccos(\mathbf{m} \cdot \mathbf{r})$ is the mismatch angle with respect to the reference mean orientation of the collagen fiber distribution $\mathbf{m}$, and the concentration parameter $b\ [0, \infty]$ describes the degree of anisotropy if b=0 represents the maximum fiber dispersion (isotropic fiber distribution). Finally, $\operatorname{erfi}(x) = -i\operatorname{erf}(x)$ denotes the

imaginary error function. A total of 5 material parameters (μ, c_1, c_2, b, θ) should be fitted.

2.3.4.2 Microfiber Bingham (MFB)

The Bingham ODF [35] was initially proposed by Alastrué et al. [33] in the formulation of a microsphere-based constitutive model introducing the anisotropy induced by fibers and its application to the modelling of arterial tissue. The dispersion of the collagen fibers with respect to their referential orientation can be written as:

$$\rho(\mathbf{r};\mathbf{A})\frac{dA}{4\pi} = [K(\mathbf{A})]^{-1}\exp(\mathbf{r}^{\mathrm{t}}\cdot\mathbf{A}\cdot\mathbf{r})\frac{dA}{4\pi} \tag{13}$$

where $\mathbf{A}$ is a symmetric order 3 matrix, dA is the Lebesgue invariant measure on the unit sphere, $\mathbf{r} \in \mathbb{U}^{\mathbf{2}}$ and $K(\mathbf{A})$ is a normalizing constant. And it can be rewritten as:

$$\rho(\mathbf{r};\mathbf{Z},\mathbf{Q})\frac{dA}{4\pi} = [F_{000}(\mathbf{Z})]^{-1}\exp\big(tr(\mathbf{Z}\cdot\mathbf{Q}^{\mathrm{t}}\cdot\mathbf{r}\cdot\mathbf{r}^{\mathrm{t}}\cdot\mathbf{Q})\big)\frac{dA}{4\pi} \tag{14}$$

where $\mathbf{Z}$ is a diagonal matrix with eigenvalues $\kappa_{1,2,3}$, $\mathbf{Q} \in \mathbb{Q}^{\mathbf{3}}$ defining the orientation of the three principal orthogonal directions relative to the reference basis, such that $\mathbf{A} = \mathbf{Q}\cdot\mathbf{Z}\cdot\mathbf{Q}^{\mathrm{t}}$ and:

$$F_{000}(\mathbf{Z}) = \frac{1}{4\pi}\int_{\mathbb{U}^{\mathbf{2}}}\exp\big(tr(\mathbf{Z}\cdot\mathbf{r}\cdot\mathbf{r}^{\mathrm{t}})\big)dA \tag{15}$$

Therefore, the probability concentration is controlled by the eigenvalues of $\mathbf{Z}$, which might be interpreted as concentration parameters. To be precise, the difference between pairs of eigenvalues $\kappa_{1,2,3}$ – i.e., $[\kappa_1 - \kappa_2]$, $[\kappa_1 - \kappa_3]$ and $[\kappa_2 - \kappa_3]$ – determines the shape of the distribution over the surface of the unit sphere. Thus, if one of these three parameters is fixed to a constant value (in this case $\kappa_3 = 0$), by varying the other two values κ_1 and κ_2, different distributions of the family of fibers might be achieved without reducing initial versatility. So, a total of 5 material parameters ($\mu, c_1, c_2, \kappa_1, \kappa_2$) should be fitted.

2.4. Fitting material parameters

Stress-stretch curves resulting from the biaxial tensile tests were used to fit five of the most widely-recognized constitutive models proposed in the literature.

Each model was fitted to biaxial test data at different ratios 1:1, 0.5:1, 1:0.5 (Figs. 4a, 6a and 8a). The tissue was assumed to be incompressible, i.e. $\det(\mathbf{F}) = \lambda_1\lambda_2\lambda_3 = 1$, where $\mathbf{F}$ is the deformation gradient tensor and $\lambda_i,\ i = 1, 2, 3$, the stretches in the principal directions. The predicted behavior obtained with each of the five models was compared with the experimental biaxial data response of two different loading protocols, 0.75:1 and 1:0.75 (not coincident with those used in the fitting), as shown in Figs. 4b, 6b and 8b, respectively. In order to quantify the predictive capability of each model, the parameters coefficient of determination R^2 and the normalized root mean square error ε_{NRMS} were evaluated. Here, ε_{NRMS} is defined as:

$$\varepsilon_{NRMS} = \frac{\sqrt{\frac{1}{n}\sum_{i=1}^{n}(X_{\exp\_i} - X_{mod\_i})^2}}{\left|\frac{1}{n}\sum_{i=1}^{n} X_{\exp\_i}\right|} \tag{16}$$

with n the number of experimental points, and $X_{\exp\_i}$ and X_{mod_i} represent the experimental and model values, respectively. So ε_{NRMS} quantifies the mean deviation between the experimental and the model data.

The five models explained above were fitted to the experimental data by means of least square optimization algorithms. A numerical Nelder-Mead method was used [36] to minimize the objective function Eq. (17) using HyperFit software [37]. This is a direct heuristic search method (based on a function comparison) using the concept of simplex and is often applied to nonlinear optimization problems. The objective function is defined as:

$$\chi^2 = \sum_{i=1}^{n}\left[\left(P_{\theta\theta} - P_{\theta\theta}^{\Psi}\right)_i^2 + \left(P_{zz} - P_{zz}^{\Psi}\right)_i^2\right] \tag{17}$$

where $P_{\theta\theta}$ and P_{zz} are the 1st Piola-Kirchhoff (engineering) stress data (3D) obtained from the tests, $P_{\theta\theta}^{\Psi} = \frac{\partial \Psi}{\partial \lambda_\theta}$ and $P_{zz}^{\Psi} = \frac{\partial \Psi}{\partial \lambda_z}$ are the 1st Piola-Kirchhoff (engineering) stress data theoretically calculated for the *i* th point for a homogeneous pure biaxial state Ψ, and *n* is the number of data points.

2.5. Statistical analysis

A statistical analysis was performed to study possible significant variations in the mechanical behavior of colonic tissue along the intestinal tract. The normal distribution of the variables was tested using the Shapiro-Wilk test. The values were divided into three groups, corresponding to the PS, DS and DC samples, and all the groups were compared by means of an independent one-tailed t-test. $p < 0.05$ was established to indicate statistical significance.

3. Results

3.1. Biaxial behavior

The colon revealed nonlinear, anisotropic and viscoelastic behavior with the apparition of hysteresis loops. However, those hysteresis loops are narrow enough to be considered as almost elastic behavior and they are not taken into account in the models proposed to describe the colonic tissue behavior.

The representative biaxial mechanical response (First Piola-Kirchhoff stress vs. stretch) is plotted in Figs. 3, 5 and 7 for PS, DS and DC, respectively. The tested specimens did not tear or exhibit signs of preliminary damage during testing. Generally, the force-controlled testing protocol allowed us to reach maximum stresses up to 60 kPa, before tearing.

Softening between subsequent stress levels was clearly visible in all specimens (Figs. 3a, 5a and 7a, respectively). The main softening occurred in the first cycles when the permanent stretch was increased. However, the elimination of this residual stretch resulted in similar material properties for each increased stress level. A typical preconditioning behavior in terms of loading-unloading cycles at maximum stress levels of 60 kPa is depicted in Figs. 3a, 5a and 7a for PS, DS and DC, respectively, which was consistent in all the tested specimens. PS shows less softening behavior than DS and DC.

The curves were stable and repeatable after a few preconditioning cycles; in particular, five cycles were enough to precondition each specimen. Figs. 3b, 5b and 7b show a representative biaxial stress test behavior with different stress ratios between the circumferential and longitudinal directions (1:1, 0.75:1, 0.5:1, 0:1, 1:0.75, 1:0.5, 1:0) for PS, DS and DC, respectively.

A plot of axial stretch versus circumferential stretch at different ratios for PS, DS and DC samples is presented in Figs. 3d, 5d and 7d, respectively, for the fifth cycle. Figs. 3c, 5c and 7c show the respective experimentally covered ranges of 1st PK stresses.

For PS specimens the maximum stretches are 1.07 and 1.05 for circumferential and longitudinal directions, respectively, for the 1:1 protocol. The homologous values for

the DS were 1.092 and 1.075, and for the DC 1.09 and 1.07. For protocol 1:0.5, we have 1.077 and 1.02 for PS, 1.118 and 1.03 for DS, and 1.12 and 1.025 for DC.

The results show high stretch values in the circumferential direction and a stiffer behavior in the longitudinal direction. These results demonstrate a progressively increasing degree of anisotropy from the proximal spiral to the descending colon. Stiffness in the longitudinal direction is maintained; however, in the circumferential direction it is progressively reduced until reaching the descending colon.

Finally, Figs. 3e-f, 5e-f and 7e-f correspond to equibiaxial 1:1 experimental data samples in circumferential (e) and longitudinal (f) directions. The plots clearly depict differences in behavior between the longitudinal and circumferential directions. For the maximum stress level (60KPa), the difference (%) of the stretch between the circumferential and longitudinal axis ranged between 1.9-5% for PS, 2.8-9% for DS, and between 1.5%-5% for DC. These results have been evaluated taking the upper and lower limit curves for stretch values in the circumferential direction and their homologous values in the longitudinal direction for the three evaluated zones. The dispersion of results observed does not reveal a clear tendency, so Figs. 3e-f, 5e-f and 7e-f include an average curve corresponding to each analyzed zone in the circumferential (e) and (f) longitudinal directions. Evaluating percentage differences in average stretches for a $P_\theta = P_z = 60KPa$ stress level, the following increments are obtained in the circumferential direction compared to the longitudinal direction: PS = 0.6%, DS = 5.8%, and DC = 4.75%. The proximal spiral shows a quasi-isotropic behavior, and both the distal spiral and the descending colon a similar degree of anisotropy. A similar dispersion of results has been observed in the three areas in both directions.

3.2. Material parameters and constitutive models comparison

The dispersion revealed by the experimental results of the tested samples show the logical impossibility of obtaining a generic model from those data. However, a general trend in the stress-strain behavior and dependence can be extracted from the results for different parts of the large intestine. The results of the fitting of material parameters that define the strain energy density function (SEF) for each of the five

analyzed models for samples from the different colonic zones (PS, DS and DC) are shown in Tables 1-3, respectively. The range of values observed for certain material parameters reflect the variation in the mechanical behavior from sample to sample. Therefore, the average values of the material parameters and the standard deviation are shown in Tables 1-3.

Material parameters have been fitted using jointly the three curves of the experimental biaxial protocols [1:1, 0.5:1 and 1:0.5] for each specimen. The coefficient of determination R^2 and the normalized root mean square error ε_{NRMS} values are included in Tables 1-3.

Each fitted model has been used to reproduce the biaxial protocols 0.75:1 and 1:0.75. The obtained curves from models have been compared to corresponding experimental data for each specimen, in order to provide a measure of prediction capability, by means of the R^2 and ε_{NRMS} included in Tables 1-3.

A first observation of the results shows that the predictive capability of SEF models corresponds to the HGO model for all positions, especially for the DS and DC samples which have a higher anisotropic behavior. The mean values for those samples were R^2<0.85 and ε_{NRMS}>0.2 ($R^2 = 0.80$, $\varepsilon_{NRMS} = 0.2277$ and $R^2 = 0.84$, $\varepsilon_{NRMS} = 0.2047$ for the DS and DC samples, respectively). For PS samples better results were obtained ($R^2 = 0.907$, $\varepsilon_{NRMS} = 0.1633$).

On the other hand, the best predictive capability corresponds to the Four Fiber Family (FFF) model showing mean values of $R^2 = 0.97$, $\varepsilon_{NRMS} = 0.0814$; $R^2 = 0.89$, $\varepsilon_{NRMS} = 0.1600$ and $R^2 = 0.94$, $\varepsilon_{NRMS} = 0.1227$ for the PS, DS and DC samples, respectively.

The orientation angles found as a result of fitting the FFF model for submucosal collagen fibers of the proximal spiral, distal spiral and descending colon have mean values of 41.1º, 46.4º and 43.17º, respectively. The spiral colon shows high standard deviation with values ranging from 32.3º to 52.6º, depending on the sample. However, the descending colon has less variation with values ranging from 37.8º to 47.2º.

Similar angle values were obtained for the HGO and Microfiber von Mises models, but for the GOH model extreme angles of 0º and 90º were obtained, without a clear physical meaning. This is because the model has a parameter which describes the level of dispersion in the fiber directions, with values near to maximum dispersion (κ = 0.33). This means that the fibers are randomly distributed and the material becomes nearly isotropic. Therefore, this angle is not significant since the fitting model describes a quasi-isotropic behavior. This may be due to the fact that the dispersion of the results of the samples masks the smooth anisotropy, reaching practically an isotropic fitting in this case, and presenting acceptable average values of R^2 and ε_{NRMS} with respect to the experimental data.

The values of parameter b for the von Mises microfiber model obtained are similar in all the samples and closer to 0.0 in the case of PS, which is consistent with the less anisotropic behavior detected in this area. However, SD and DC show higher values, indicating a greater directionality of the fibers (low dispersion) and therefore a more anisotropic behavior.

The Bingham microfiber model has very high similar κ_1 and κ_2 values, which indicates a distribution of fibers contained in a dominant plane.

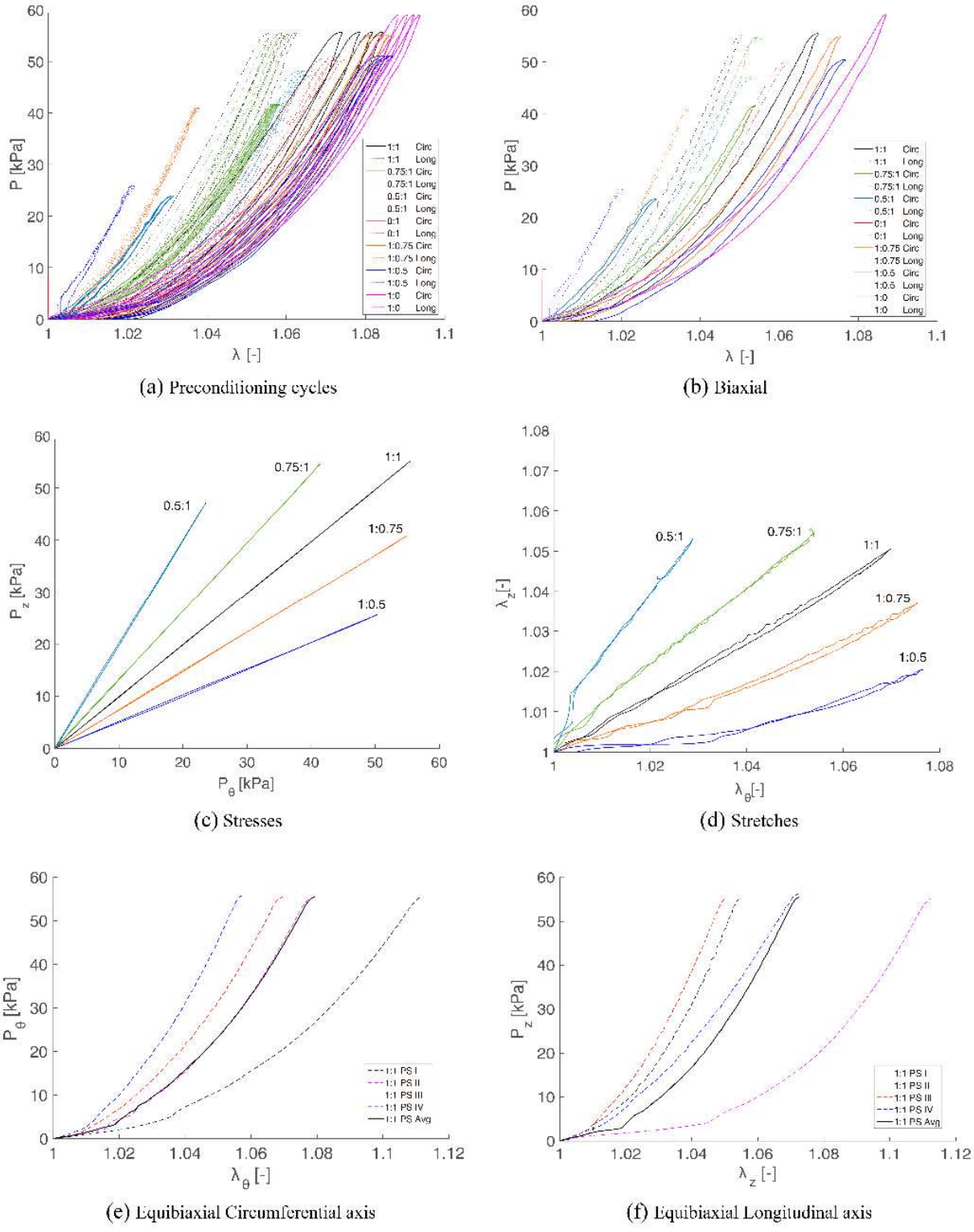

Fig. 3. Representative (specimen PS III) 1st Piola-Kirchhoff stress vs. stretch behavior for the proximal parts of porcine spiral colon specimens: (a) preconditioning behavior in terms of loading-unloading cycles at 60 [kPa]; (b) biaxial behavior at different ratios (Circ axis : Long axis) 1:1, 0.5:1, 1:0.5, 0.75:1, 1: 0.75, 0:1, 1:0; (c) Plots showing experimentally covered ranges of 1st PK stresses and (d) stretches of a typical sample; (e) equibiaxial 1:1 experimental data samples in circumferential and (f) longitudinal directions.

Table 1. Material parameters for the Proximal Spiral colon specimens (PS) for each analyzed model, along with average (Mean) and standard deviation (SD).

									Fitting 1:1, 0.5:1 and 1:0.5		Predicting 0.75:1 and 1:0.75	
HGO model												
Specimen	μ [kPa]	k_1 [kPa]	k_2 [-]	θ [º]					R^2 [-]	ε_{NRMSE} [-]	R^2 [-]	ε_{NRMSE} [-]
PS I	59.4452	20.2270	58.1421	49.52					0.8027	0.2440	0.9186	0.1622
PS II	20.1180	30.6340	34.2500	43.54					0.7167	0.2692	0.8689	0.1858
PS III	44.3680	45.8780	103.9260	45.72					0.7626	0.2506	0.9193	0.1602
PS IV	105.751	15.8220	129.1080	48.70					0.8326	0.2234	0.9233	0.1451
Mean	57.4206	28.1402	81.3565	46.87					0.7787	0.2468	0.9075	0.1633
SD	31.2321	11.5673	37.2408	2.38					0.0435	0.0164	0.0224	0.0146
GOH model												
Specimen	μ [kPa]	k_1 [kPa]	k_2 [-]	κ [-]	θ [º]				R^2 [-]	ε_{NRMSE} [-]	R^2 [-]	ε_{NRMSE} [-]
PS I	19.4105	2313.3107	0.001	0.3196	89.46				0.8685	0.1832	0.9579	0.1104
PS II	4.8060	2355.4320	0.001	0.3200	0.00				0.7964	0.2110	0.8958	0.1788
PS III	40.9900	4774.8573	0.001	0.3266	89.99				0.8749	0.1763	0.9388	0.1181
PS IV	42.7710	3334.2850	0.001	0.3240	0.00				0.9031	0.1648	0.9594	0.1079
Mean	26.9944	3194.4712	0.0010	0.3226	--				0.8607	0.1838	0.9379	0.1288
SD	15.7688	999.6998	0.0000	0.0029	--				0.0393	0.0170	0.0257	0.0291
Four Fiber Family model												
Specimen	μ [kPa]	k_{11} [kPa]	k_{21} [-]	k_{12} [kPa]	k_{22} [-]	$k_{13}=k_{14}$ [kPa]	$k_{23}=k_{24}$ [-]	θ [º]	R^2 [-]	ε_{NRMSE} [-]	R^2 [-]	ε_{NRMSE} [-]
PS I	3.0609	100.5361	65.1690	17.7940	17.3431	88.2790	22.6840	40.51	0.9760	0.0845	0.9812	0.0761
PS II	0.1010	13.7740	29.5251	110.2720	27.9420	39.1730	25.8280	55.81	0.9717	0.0936	0.9634	0.1014
PS III	7.3550	164.9000	70.2312	12.5430	15.6364	146.4790	33.5900	32.31	0.9741	0.0870	0.9856	0.0698
PS IV	3.1150	131.9790	7.6870	3.8580	137.6820	190.9040	30.5200	35.81	0.9585	0.1115	0.9812	0.0781
Mean	3.4080	102.7973	43.1531	36.1168	49.6509	116.2088	28.1555	41.11	0.9701	0.0941	0.9779	0.0814
SD	2.5846	56.2107	25.7948	43.1018	51.0430	57.4679	4.1976	8.97	0.0069	0.0106	0.0085	0.0120
Microfiber Von Mises model												
Specimen	μ [kPa]	c_1 [kPa]	c_2 [-]	b [-]	θ [º]				R^2 [-]	ε_{NRMSE} [-]	R^2 [-]	ε_{NRMSE} [-]
PS I	25.0310	85.1160	39.8920	2.9340	58.56				0.9582	0.1158	0.9553	0.1175
PS II	5.0000	62.1530	48.0550	1.7650	30.88				0.9425	0.1393	0.7907	0.2129
PS III	12.2820	235.0890	47.2700	1.5200	53.34				0.9666	0.0979	0.9828	0.0767
PS IV	11.4400	167.3760	34.8750	3.2660	41.83				0.9332	0.1301	0.9619	0.1044
Mean	13.4383	137.4335	42.5230	2.3713	46.15				0.9501	0.1207	0.9227	0.1279
SD	7.2616	68.6247	5.4441	0.7432	10.69				0.0131	0.0156	0.0769	0.0512
Microfiber Bingham model												
Specimen	μ [kPa]	c_1 [kPa]	c_2 [-]	κ_1 [-]	κ_2 [-]				R^2 [-]	ε_{NRMSE} [-]	R^2 [-]	ε_{NRMSE} [-]
PS I	23.9370	89.5020	26.1110	9.4280	11.4330				0.9426	0.1395	0.9583	0.1157
PS II	8.4780	48.0200	34.5780	15.6470	14.1800				0.9655	0.1037	0.9176	0.1274
PS III	18.6710	448.8732	2.6564	0	0.5539				0.9339	0.1498	0.9287	0.1564
PS IV	8.0120	156.1149	16.4626	28.5196	28.1548				0.8153	0.2111	0.9619	0.1044
Mean	14.7745	185.6275	19.9520	13.3987	13.5804				0.9143	0.1510	0.9416	0.1260
SD	6.7918	156.8002	11.8656	10.3560	9.8371				0.0583	0.0386	0.0189	0.0194

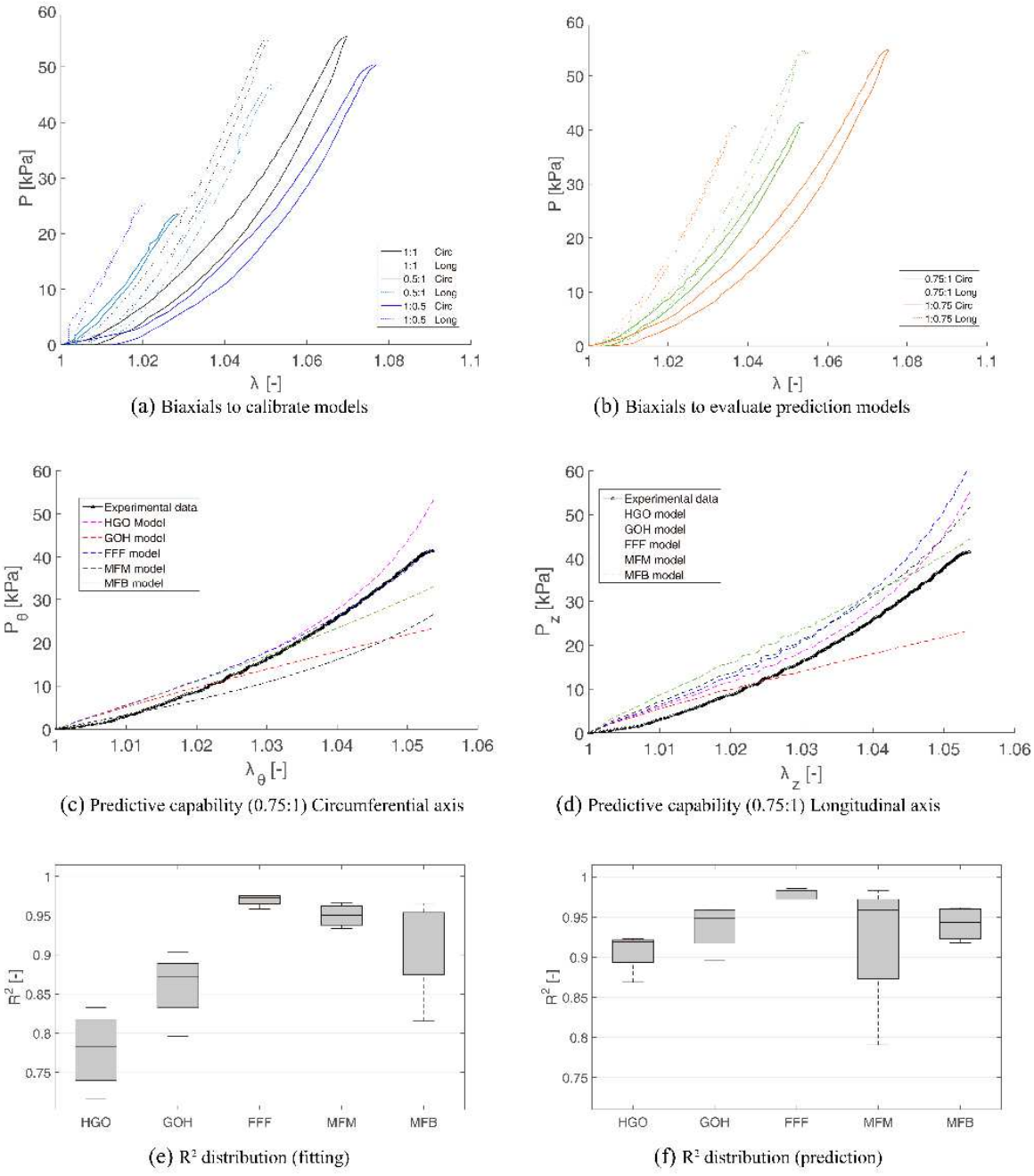

(a) Biaxials to calibrate models

(b) Biaxials to evaluate prediction models

(c) Predictive capability (0.75:1) Circumferential axis

(d) Predictive capability (0.75:1) Longitudinal axis

(e) R^2 distribution (fitting)

(f) R^2 distribution (prediction)

Fig. 4. Representative plot of predictive capability of the analyzed constitutive models for a typical behavior for the proximal parts of porcine spiral colon (specimen PS III). All the models were fitted to biaxial test data at different ratios 1:1, 0.5:1, 1:0.5 and then their predicted biaxial response to 2 different loading protocols 0.75:1 and 1:0.75 was compared with experimental data: (a) biaxial experimental data behavior after preconditioning cycle at ratios 1:1, 0.5:1, 1:0.5 used for the 5 proposed model calibrations; (b) biaxial experimental data protocols 0.75:1 and 1:0.75 to compare the behavior prediction given by the 5 models; (c) biaxial 0.75:1 protocol to compare predictive results vs experimental data in circumferential and (d) longitudinal direction; (e) Descriptive capability of the 5 constitutive models: comparative results (R^2) of each fitted constitutive model to capture the measured biaxial response (protocols 1:1, 0.5:1 and 1:0.5) of proximal parts of porcine spiral colon; (f) Predictive capability of the 5 constitutive models: comparative results (R^2) of each fitted constitutive model to predict the biaxial response (protocols 0.75:1 and 1:0.75) of proximal parts of porcine spiral colon.

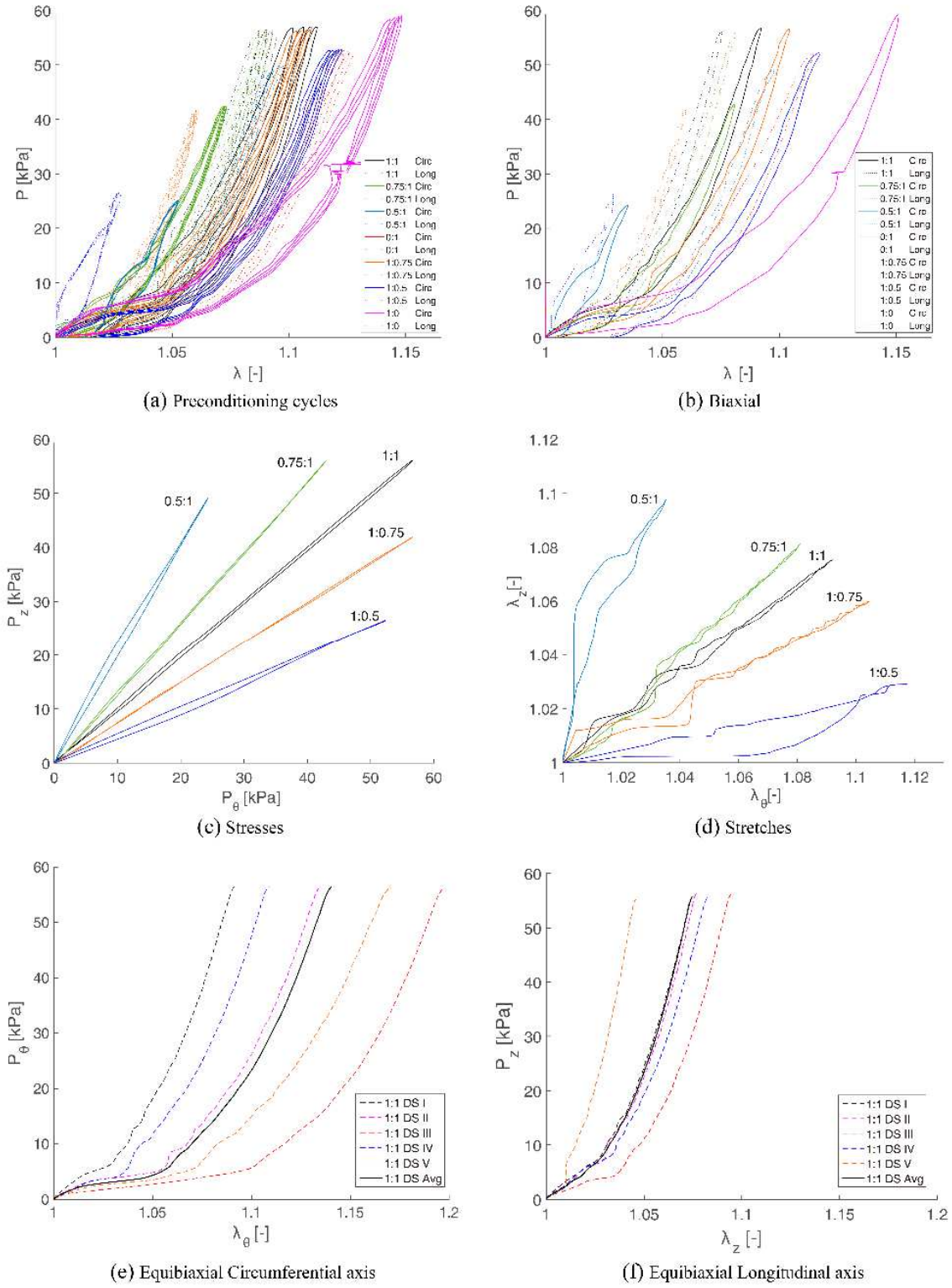

Fig. 5. Representative (specimen DS I) 1st Piola-Kirchhoff stress vs. stretch behavior for the distal parts of porcine spiral colon specimens: (a) preconditioning behavior in terms of loading-unloading cycles at 60 [kPa]; (b) biaxial behavior at different ratios (Circ axis : Long axis) 1:1, 0.5:1, 1:0.5, 0.75:1, 1: 0.75, 0:1, 1:0; (c) Plots showing experimentally covered ranges of 1st PK stresses and (d) stretches of a typical sample; (e) equibiaxial 1:1 experimental data samples in circumferential and (f) longitudinal directions.

Table 2. Material parameters for the Distal Spiral colon specimens (DS) for each analyzed model, along with average (Mean) and standard deviation (SD).

									Fitting 1:1, 0.5:1 and 1:0.5		Predicting 0.75:1 and 1:0.75	
HGO model												
Specimen	μ [kPa]	k_1 [kPa]	k_2 [-]	θ [º]					R^2 [-]	ε_{NRMSE} [-]	R^2 [-]	ε_{NRMSE} [-]
DS I	62.8480	10.9211	73.2590	46.64					0.8232	0.2251	0.8754	0.1765
DS II	44.5462	16.0596	42.0310	48.47					0.8156	0.2274	0.9177	0.1555
DS III	41.8570	4.2541	28.0443	50.94					0.6743	0.3184	0.6914	0.3158
DS IV	38.2527	8.7432	55.0785	45.95					0.7006	0.2846	0.8193	0.2093
DS V	43.7351	15.2372	46.6890	52.83					0.7583	0.2610	0.6908	0.2816
Mean	46.2478	11.0430	49.0204	48.96					0.7544	0.2633	0.7989	0.2277
SD	8.5788	4.3394	14.9566	2.59					0.0597	0.0353	0.0934	0.0614
GOH model												
Specimen	μ [kPa]	k_1 [kPa]	k_2 [-]	κ [-]	θ [º]				R^2 [-]	ε_{NRMSE} [-]	R^2 [-]	ε_{NRMSE} [-]
DS I	15.8550	3017.3426	0.01	0.3300	89.93				0.8824	0.1543	0.9071	0.1349
DS II	8.8319	1570.4851	114.118	0.3200	89.99				0.8859	0.1481	0.9693	0.0784
DS III	11.6322	523.9737	0.001	0.3160	89.99				0.7454	0.2727	0.8312	0.2251
DS IV	14.4270	1702.6370	0.01	0.3330	89.32				0.7966	0.2301	0.9001	0.1538
DS V	10.9957	1141.1080	0.01	0.3070	89.67				0.7000	0.2296	0.7259	0.2518
Mean	12.3484	1591.1093	22.8298	0.3212	89.78				0.8021	0.2070	0.8667	0.1688
SD	2.5030	823.1992	45.6441	0.0095	0.26				0.0737	0.0482	0.0829	0.0626
Four Fiber Family model												
Specimen	μ [kPa]	k_{11} [kPa]	k_{21} [-]	k_{12} [kPa]	k_{22} [-]	$k_{13}=k_{14}$ [kPa]	$k_{23}=k_{24}$ [-]	θ [º]	R^2 [-]	ε_{NRMSE} [-]	R^2 [-]	ε_{NRMSE} [-]
DS I	4.4198	53.6151	15.3170	64.2110	7.9490	67.8232	41.7690	47.67	0.9759	0.0707	0.9468	0.0943
DS II	3.2870	40.7893	20.5125	28.4687	5.4111	62.7480	29.3791	47.84	0.9729	0.0908	0.9491	0.1164
DS III	27.8910	0.1490	47.1046	41.5059	0.0101	16.5769	47.1050	89.99	0.6417	0.3076	0.7698	0.2529
DS IV	2.9408	64.7509	22.6780	61.8451	0.0267	40.2280	23.2473	37.64	0.8316	0.2341	0.9493	0.1285
DS V	10.6090	32.2380	139.6419	27.2159	3.7140	52.6283	33.0361	52.60	0.9588	0.1156	0.8349	0.2078
Mean	9.8295	38.3085	49.0508	44.6493	3.4222	48.0009	34.9073	55.15	0.8762	0.1637	0.8900	0.1600
SD	9.4483	22.0574	46.6014	15.8365	3.0888	18.3287	8.5544	18.09	0.1289	0.0916	0.0744	0.0602
Microfiber Von Mises model												
Specimen	μ [kPa]	c_1 [kPa]	c_2 [-]	b [-]	θ [º]				R^2 [-]	ε_{NRMSE} [-]	R^2 [-]	ε_{NRMSE} [-]
DS I	5.9235	87.2130	31.6210	3.6787	47.15				0.9706	0.0975	0.9810	0.0762
DS II	29.9570	27.4451	39.8286	10.0950	52.25				0.9102	0.1497	0.9367	0.1270
DS III	19.5492	50.1733	14.9151	1.4363	89.95				0.7464	0.2781	0.7589	0.2668
DS IV	3.5040	97.6110	24.4160	2.0531	48.93				0.9643	0.1066	0.6882	0.2603
DS V	3.6971	15.1478	13.0984	3.1930	61.65				0.8785	0.1883	0.7622	0.2628
Mean	12.5262	55.5180	24.7758	4.0912	59.99				0.8940	0.1640	0.8254	0.1986
SD	10.5461	32.3197	10.0714	3.1056	15.80				0.0814	0.0656	0.1130	0.0808
Microfiber Bingham model												
Specimen	μ [kPa]	c_1 [kPa]	c_2 [-]	κ_1 [-]	κ_2 [-]				R^2 [-]	ε_{NRMSE} [-]	R^2 [-]	ε_{NRMSE} [-]
DS I	6.6764	85.0973	19.0718	20.6261	20.9594				0.9202	0.1542	0.9742	0.0880
DS II	27.1623	66.2180	7.4431	25.1645	26.6451				0.7902	0.2630	0.8208	0.2407
DS III	31.9270	21.1689	16.8911	25.9654	29.6680				0.7964	0.2609	0.8247	0.2364
DS IV	6.2567	61.9283	21.8431	20.9546	21.4588				0.9475	0.1222	0.7411	0.2459
DS V	9.6260	94.7143	8.0223	24.7374	27.3754				0.8887	0.1940	0.8400	0.2241
Mean	16.3297	65.8254	14.6543	23.4896	25.2213				0.8686	0.1988	0.8401	0.2070
SD	10.9564	25.3595	5.8682	2.2413	3.4282				0.0643	0.0563	0.0754	0.0600

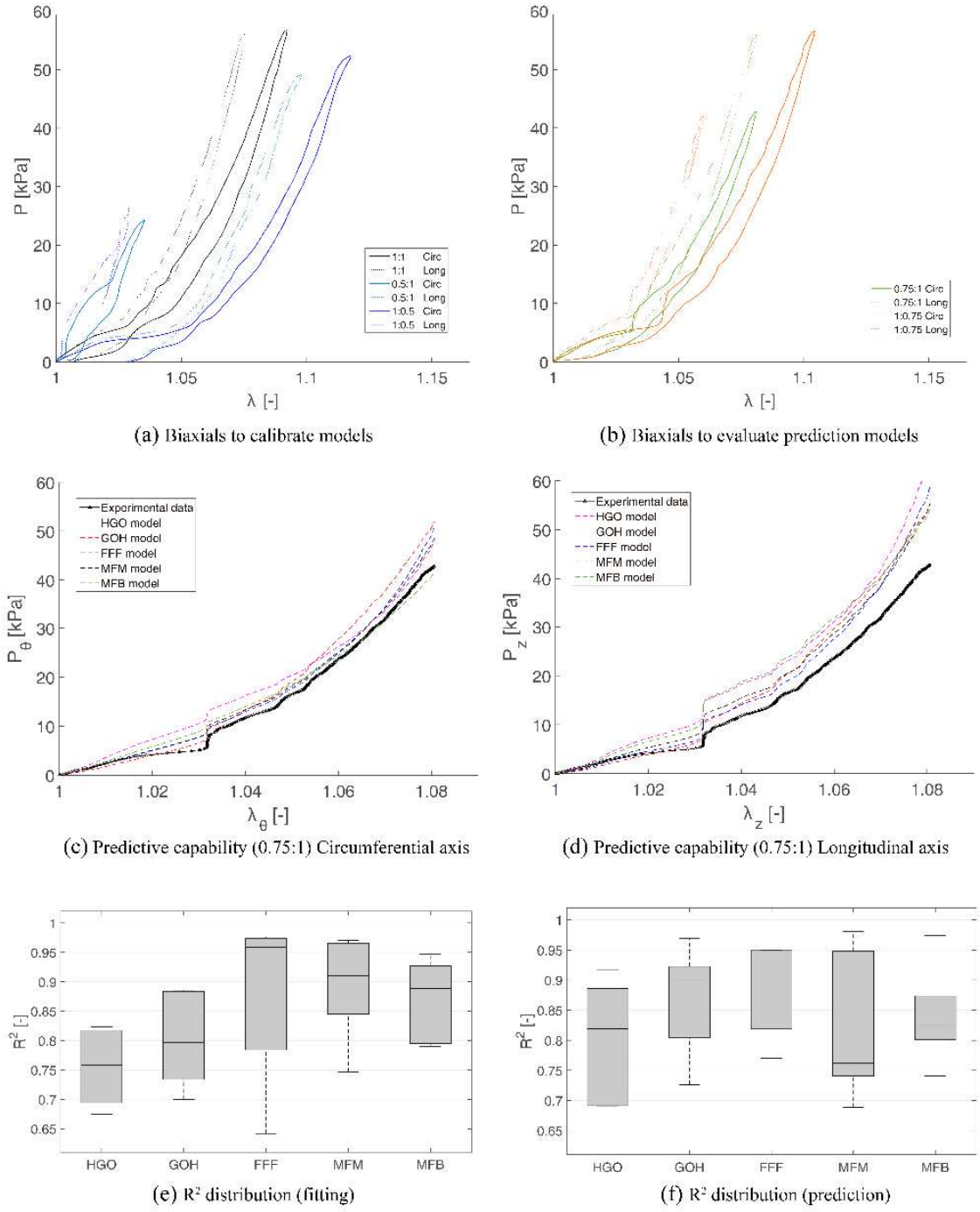

Fig. 6. Representative plot of predictive capability of the analyzed constitutive models for a typical behavior for the distal parts of porcine spiral colon (specimen DS I). All the models were fitted to biaxial test data at different ratios 1:1, 0.5:1, 1:0.5 and then their predicted biaxial response to 2 different loading protocols 0.75:1 and 1:0.75 was compared with experimental data: (a) biaxial experimental data behavior after preconditioning cycle at ratios 1:1, 0.5:1, 1:0.5 used for the 5 proposed model calibrations; (b) biaxial experimental data protocols 0.75:1 and 1:0.75 to compare the behavior prediction given by the 5 models; (c) biaxial 0.75:1 protocol to compare predictive results vs experimental data in circumferential and (d) longitudinal direction; (e) Descriptive capability of the 5 constitutive models: comparative results (R^2) of each fitted constitutive model to capture the measured biaxial response (protocols 1:1, 0.5:1 and 1:0.5) of proximal parts of porcine spiral colon; (f) Predictive capability of the 5 constitutive models: comparative results (R^2) of each fitted constitutive model to predict the biaxial response (protocols 0.75:1 and 1:0.75) of proximal parts of porcine spiral colon.

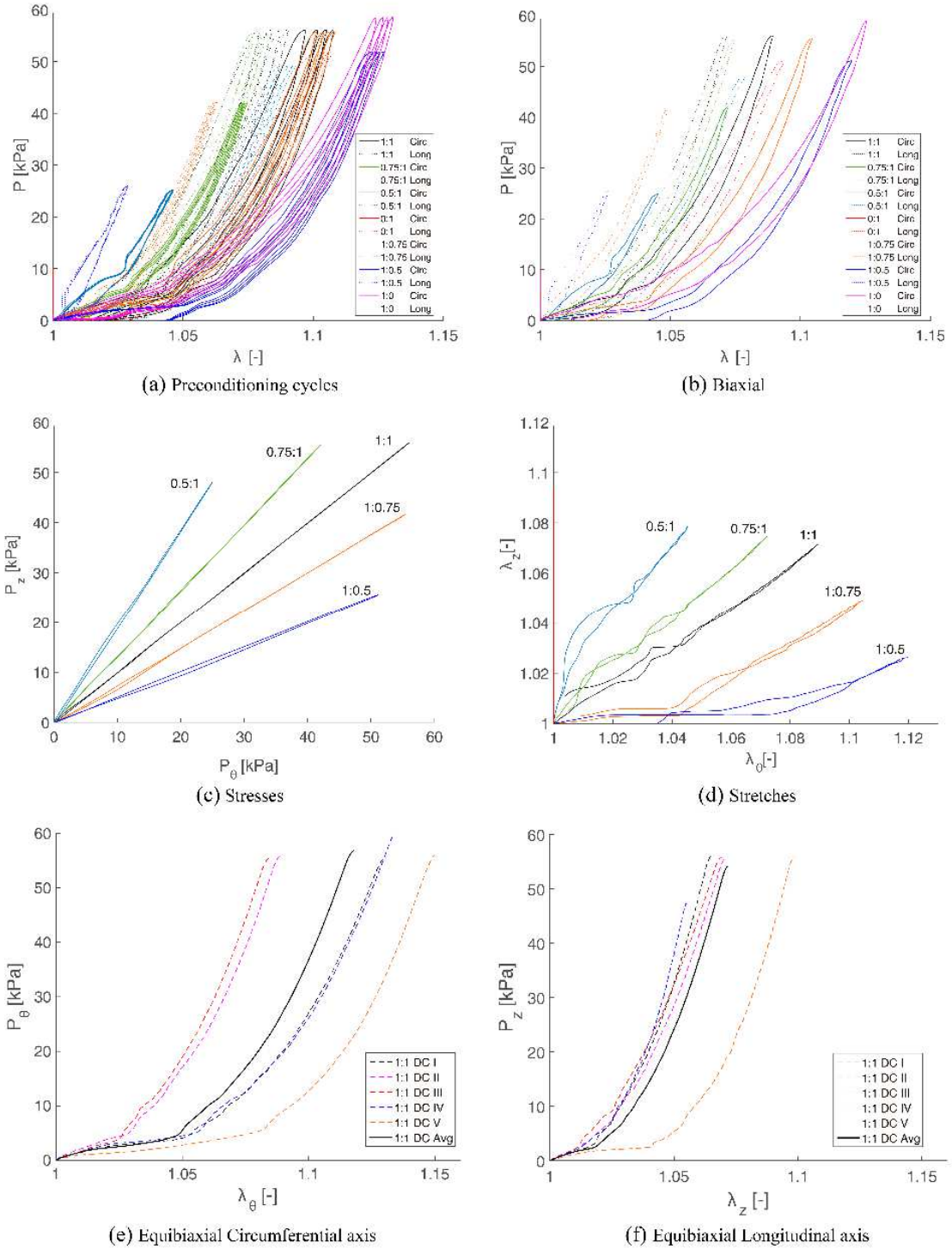

Fig. 7. Representative (specimen DC II) 1st Piola-Kirchhoff stress vs. stretch behavior for porcine descending colon specimens: (a) preconditioning behavior in terms of loading-unloading cycles at 60 [kPa]; (b) biaxial behavior at different ratios (Circ axis : Long axis) 1:1, 0.5:1, 1:0.5, 0.75:1, 1: 0.75, 0:1, 1:0; (c) Plots showing experimentally covered ranges of 1st PK stresses and (d) stretches of a typical sample; (e) equibiaxial 1:1 experimental data samples in circumferential and (f) longitudinal directions.

Table 3. Material parameters for the Descending Colon specimens (DC) for each analyzed model, along with average (Mean) and standard deviation (SD).

									Fitting 1:1, 0.5:1 and 1:0.5		Predicting 0.75:1 and 1:0.75	
HGO model												
Specimen	μ [kPa]	k_1 [kPa]	k_2 [-]	θ [º]					R^2 [-]	ε_{NRMSE} [-]	R^2 [-]	ε_{NRMSE} [-]
DC I	40.6322	16.7518	44.5265	48.42					0.7534	0.2647	0.8987	0.1804
DC II	36.5595	38.5816	44.0640	47.45					0.8705	0.1866	0.9241	0.1544
DC III	72.6798	17.2810	66.6798	45.87					0.8496	0.2125	0.9168	0.1637
DC IV	14.9011	10.6687	60.7227	43.84					0.6811	0.3020	0.6260	0.3306
DC V	17.9258	9.2812	32.8583	46.73					0.6945	0.2808	0.8529	0.1947
Mean	36.5397	18.5129	49.7703	46.46					0.7698	0.2493	0.8437	0.2047
SD	20.6764	10.5274	12.2635	1.56					0.0779	0.0431	0.1116	0.0644
GOH model												
Specimen	μ [kPa]	k_1 [kPa]	k_2 [-]	κ [-]	θ [º]				R^2 [-]	ε_{NRMSE} [-]	R^2 [-]	ε_{NRMSE} [-]
DC I	7.6383	1887.1271	0.179616	0.3204	90.00				0.7928	0.2076	0.9533	0.1218
DC II	16.0708	3091.3800	0.013461	0.3255	90.00				0.9458	0.1182	0.9590	0.1001
DC III	26.0342	3297.4191	0.001	0.3300	90.00				0.9368	0.1320	0.9656	0.1021
DC IV	17.7803	11.2590	47.2009	0.0000	41.94				0.7147	0.2581	0.8224	0.2171
DC V	1.7693	729.2622	159.3817	0.3223	85.37				0.7541	0.2258	0.8592	0.1805
Mean	13.8586	1803.2895	41.3554	0.2596	79.46				0.8288	0.1884	0.9119	0.1443
SD	8.4067	1285.5767	61.7725	0.1299	18.85				0.0951	0.0543	0.0593	0.0466
Four Fiber Family model												
Specimen	μ [kPa]	k_{11} [kPa]	k_{21} [-]	k_{12} [kPa]	k_{22} [-]	$k_{13}=k_{14}$ [kPa]	$k_{23}=k_{24}$ [-]	θ [º]	R^2 [-]	ε_{NRMSE} [-]	R^2 [-]	ε_{NRMSE} [-]
DC I	16.3396	69.8095	61.8184	16.8650	0.0639	27.5047	32.2740	37.86	0.9455	0.1226	0.9279	0.1523
DC II	7.6860	61.1610	34.9920	74.8340	2.5770	54.2910	51.5760	47.21	0.9503	0.1240	0.9809	0.0782
DC III	7.3264	67.3851	32.4355	19.4257	32.9646	109.4537	30.5541	42.10	0.9802	0.0798	0.9887	0.0619
DC IV	7.8120	51.7360	50.6680	27.5171	8.5570	29.8450	42.8130	44.29	0.9804	0.0812	0.8643	0.1891
DC V	11.7420	19.0057	40.3961	20.0796	3.4725	6.2925	42.9804	44.41	0.9343	0.1451	0.9469	0.1318
Mean	10.1812	53.8194	44.0620	31.7443	9.5270	45.4774	40.0395	43.17	0.9581	0.1106	0.9417	0.1227
SD	3.4742	18.4929	10.8610	21.8348	12.0397	35.4217	7.7422	3.11	0.0188	0.0258	0.0446	0.0470
Microfiber Von Mises model												
Specimen	μ [kPa]	c_1 [kPa]	c_2 [-]	b [-]	θ [º]				R^2 [-]	ε_{NRMSE} [-]	R^2 [-]	ε_{NRMSE} [-]
DC I	8.7240	73.6395	28.2483	3.4121	57.39				0.9036	0.1717	0.9395	0.1392
DC II	7.6589	88.8636	32.0682	3.4929	51.15				0.8812	0.1999	0.9404	0.1358
DC III	8.8831	109.5239	35.7969	3.3008	48.03				0.9785	0.0827	0.9879	0.0633
DC IV	7.1726	60.8699	25.9966	4.7301	51.17				0.8541	0.1812	0.8629	0.1970
DC V	10.7740	16.0397	32.7274	7.4692	53.13				0.8340	0.2090	0.7846	0.2138
Mean	8.6425	69.7873	30.9675	4.4810	52.17				0.8903	0.1689	0.9031	0.1498
SD	1.2439	31.3881	3.4565	1.5813	3.08				0.0500	0.0451	0.0715	0.0531
Microfiber Bingham model												
Specimen	μ [kPa]	c_1 [kPa]	c_2 [-]	κ_1 [-]	κ_2 [-]				R^2 [-]	ε_{NRMSE} [-]	R^2 [-]	ε_{NRMSE} [-]
DC I	7.8667	91.4500	14.4029	9.7448	11.5473				0.8819	0.1968	0.8968	0.1826
DC II	7.8296	112.6515	6.2376	13.6653	14.2236				0.8507	0.1880	0.8828	0.1994
DC III	8.3193	111.2712	16.6386	22.1284	22.4134				0.8654	0.1958	0.9260	0.1561
DC IV	1.4008	78.0271	16.1766	12.5735 38	14.3098				0.8350	0.2349	0.8961	0.1771
DC V	7.2616	43.4192	11.8627	10.8312	12.5500				0.7643	0.2840	0.8250	0.2410
Mean	6.5356	87.3638	13.0637	13.7887	15.0088				0.8395	0.2199	0.8853	0.1912
SD	2.5892	25.4795	3.8027	4.3850	3.8460				0.0407	0.0360	0.0333	0.0285

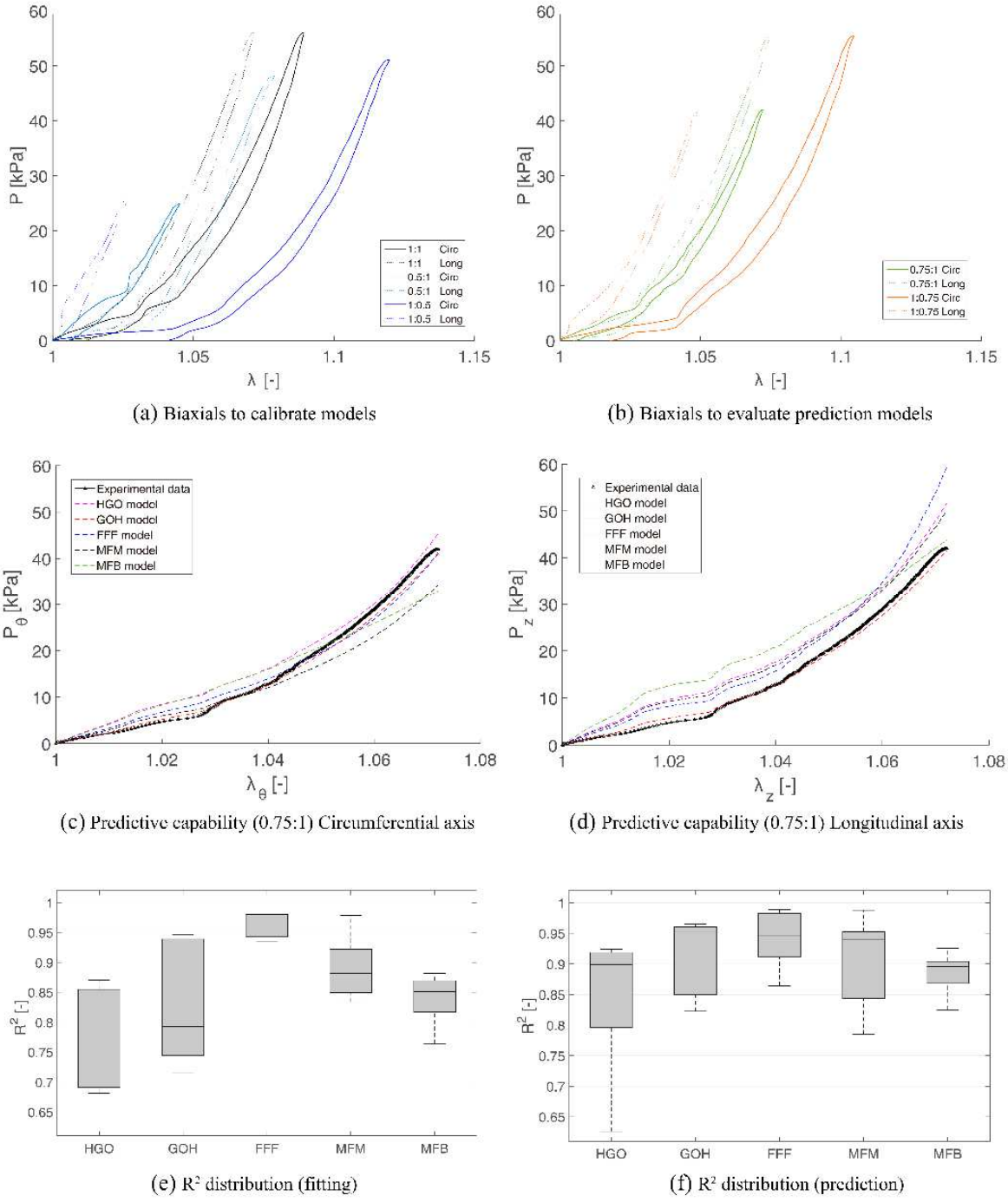

(a) Biaxials to calibrate models

(b) Biaxials to evaluate prediction models

(c) Predictive capability (0.75:1) Circumferential axis

(d) Predictive capability (0.75:1) Longitudinal axis

(e) R^2 distribution (fitting)

(f) R^2 distribution (prediction)

Fig. 8. Representative plot of predictive capability of the analyzed constitutive models for a typical behavior for porcine descending colon (specimen DC II). All the models were fitted to biaxial test data at different ratios 1:1, 0.5:1, 1:0.5 and then their predicted biaxial response to 2 different loading protocols 0.75:1 and 1:0.75 was compared with experimental data: (a) biaxial experimental data behavior after preconditioning cycle at ratios 1:1, 0.5:1, 1:0.5 used for the 5 proposed model calibrations; (b) biaxial experimental data protocols 0.75:1 and 1:0.75 to compare the behavior prediction given by the 5 models; (c) biaxial 0.75:1 protocol to compare predictive results vs experimental data in circumferential and (d) longitudinal direction; (e) Descriptive capability of the 5 constitutive models: comparative results (R^2) of each fitted constitutive model to capture the measured biaxial response (protocols 1:1, 0.5:1 and 1:0.5) of proximal parts of porcine spiral colon; (f) Predictive capability of the 5 constitutive models: comparative results (R^2) of each fitted constitutive model to predict the biaxial response (protocols 0.75:1 and 1:0.75) of proximal parts of porcine spiral colon.

Finally, Fig. 9 shows the comparison among PS, DS and DC zones where a variation of the flexibility in circumferential direction is observed. In longitudinal direction the variations of mechanical response are practically negligible.

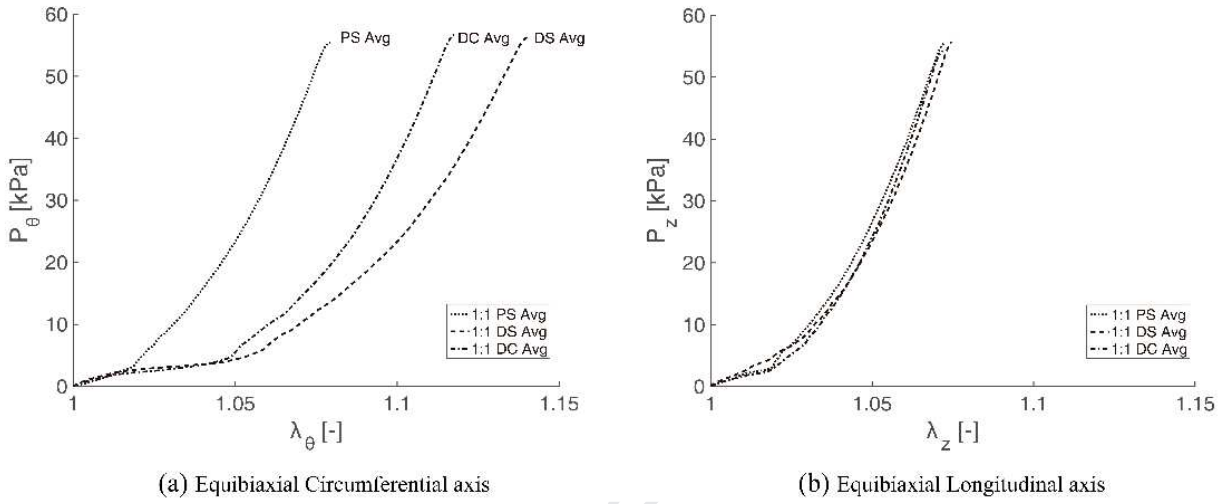

(a) Equibiaxial Circumferential axis (b) Equibiaxial Longitudinal axis

Fig. 9. Influence of colon region on the mechanical response. Comparison of average curves obtained for each zone: (a) Equibiaxial response in circumferential direction; (b) Equibiaxial response in longitudinal direction.

3.3. Statistical analysis

The mechanical properties for the PS, DS and DC were compared for both circumferential and longitudinal directions. The values were divided into three groups corresponding to the PS, DS and DC samples, and all the groups were compared. These values correspond to 25 and 50 kPa of engineering stress. Anisotropy was analyzed by the difference in circumferential and longitudinal stretches divided by their average value (Table 4).

The statistical analysis revealed significant differences between the mechanical behavior from PS to DS and DC samples in circumferential direction ($p<0.05$) at virtually any stress level. In contrast, the longitudinal tests show similar stress-stretch curves for all locations. The anisotropic parameter of PS tissue is significantly lower ($p<0.05$) and closer to 0 than the anisotropic parameters for DS and DC tissue for all stress levels. This fact demonstrates that PS tissue is more isotropic than DS and DC.

Table 4. Circumferential (λ_ϑ^{25}, λ_ϑ^{50}) and longitudinal (λ_z^{25}, λ_z^{50}) stretches and anisotropy measurements corresponding to 25 kPa and 50 kPa during equibiaxial test (1:1), respectively. Anisotropy (A^{25}, A^{50}) was analyzed by the difference in circumferential and longitudinal stretches at each stress level (25 kPa and 50 kPa respectively) divided by their average value. Values are presented as Mean ± Standard Deviation.

Specimens	λ_ϑ^{25}	λ_z^{25}	A^{25}	λ_ϑ^{50}	λ_z^{50}	A^{50}
PS	1.052 ± 0.016	1.049 ± 0.022	0.003 ± 0.026	1.074 ± 0.019	1.068 ± 0.024	0.006 ± 0.031
DS	1.103 ± 0.034	1.052 ± 0.013	0.047 ± 0.032	1.133 ± 0.038	1.070 ± 0.016	0.056 ± 0.036
DC	1.087 ± 0.024	1.051 ± 0.013	0.034 ± 0.017	1.111 ± 0.025	1.069 ± 0.013	0.039 ± 0.020

4. Discussion

The objective in this work was to obtain appropriate useful information about the colon mechanical response in order to fit the elastic parameters of different specialized behavior models. These material parameters allow us to do reliable simulations in which the role played by the colonic tissue is essential, as for example colonic stent design.

To achieve this objective, this paper aims to study and better understand the mechanical properties of pig colon tissue, selected because its physiological similarity to human tissue. To demonstrate any possible position-related difference, the study analyzed and compared the biaxial mechanical properties of different parts, focusing on the proximal spiral colon (PS), distal spiral colon (DS) and descending colon (DC) stemming from the same porcine subjects. Based on the experimental obtained results, the values of elastic parameters for five well-known constitutive models with different strain energy functions (SEF) were fitted, showing how these mechanical properties are affected by location along the colon.

Hysteresis loops were relatively narrow, i.e. the specimens behaved nearly elastically. However, all samples were preconditioned with initial loading-unloading cycles. Specifically, five cycles were enough to precondition all the tissue samples independently of the zone (PS, DS and DC) before processing the results.

We found that the nature of the porcine colon changed from a more isotropic to a more anisotropic tissue and became progressively more flexible and compliant in

circumferential direction depending on the position along the duct as it approaches the rectum (Fig. 9). Significant differences in the anisotropy parameters between the PS, DS and DC samples were observed (Table 4). The PS samples showed an overall quasi-isotropic behavior.

The orientation angles found after fitting the FFF model for submucosal collagen fibers of the proximal spiral, distal spiral and descending colon had mean values of 41.1°, 46.4° and 43.17°, respectively. Spiral colon shows a high standard deviation with values ranging from 32.3° to 52.6°, depending on the sample. However, descending colon has less variation with values ranging from 37.8° to 47.2°. These values are similar to those presented in previous colon studies obtained from extension-inflation tests [12], and somewhat higher than the 31.3° [11] estimated from uniaxial tests.

In view of the fitting results obtained in this work, it is possible to establish a comparison of the capability of prediction of the five selected constitutive models, some with a phenomenological approach and others being structural models providing a more physiological description through their material parameters. It can be seen that the four fiber family model (FFF) provides the best prediction independently of the colon location analyzed. Furthermore, the fibers can be associated with the layered structure of the tissue. There is a direct correlation between the fiber families' orientation and the physiological structure (Fig 1.b).

On the other hand, the HGO and GHO models provide acceptable results for proximal spiral colon specimens, which have a lower degree of anisotropy. The values of the orientation angles obtained in the GHO model do not have a clear physiological meaning, because the fitting parameter κ reaches values around 0.33 corresponding to the maximum dispersion of the fibers, describing a quasi-isotropic behavior. The fiber angle is therefore irrelevant.

The results confirm that the FFF model used with a similar formulation to models presented in Natali et al. (2009) [38], Ciarletta et al. (2009) [10], Sokoli et al. (2011) [14], and Patel et al. (2018) [12] are the most suitable for modeling this type of tissue.

However, this model has more material parameters than the other analyzed models, which would be a disadvantage for numerical simulation, involving a higher computational cost. Microfiber models used for the modeling of vascular tissues [33, 34] do not provide better results, because colon tissue has a lower fiber orientation dispersion than arteries [12].

One of the main limitations of the present study is the use of frozen samples, which can affect the passive mechanical properties of the tissue. Despite structural differences between human and porcine colonic tissues [39], there is consensus that porcine tissues are suitable for a first approach towards developing test models and increasing the understanding of the biomechanical behavior of the human colon. This is due to both their size and functional similarities, as well as the ease of procurement of porcine tissue. Experimental tests were performed on samples with the whole structure of the tissue, without dissection by layers. We would emphasize the need for further studies involving layer-specific mechanical tests and micro-structured constitutive models that take into account experimental data obtained from histological analysis with the help of advanced microscopic imaging.

5. Conclusion

Our results showed that the excised porcine colon is non-linear and anisotropic with the circumferential direction being more compliant. When comparing PS, DS and DC, we found statistically significant differences for the stiffness of PS tissues, being stiffer in the circumferential direction and that they display a quasi-isotropic behavior. The tissue along the colon changed from being more isotropic to being more anisotropic and became progressively more flexible in the circumferential direction. However, the same stiffness in the longitudinal direction towards the rectum is maintained.

In conclusion, the analyzed models, with the fitted elastic parameters, may be used for more realistic and reliable FE simulations, providing an appropriate framework for the design of optimal devices for the treatment of colonic diseases. In this respect, the four fiber family model (FFF) provides the best prediction independently of the colon

location analyzed. This model would therefore be the most appropriate for simulating the mechanical behavior of colonic tissue.

List of abbreviations

DC: Descending colon

DIC: Digital image correlation

DS: Distal spiral colon

FFF: Four fiber family model

GOH: Gasser-Ogden-Holzapfel model

HGO: Holzapfel-Gasser-Ogden model

MFB: Microfiber Bingham model

MFM: Microfiber von Mises model

ODF: Orientation density function

PS: Proximal spiral colon

PSS: Physiological saline solution

SEF: Strain energy function

Competing interest

This research did not receive any specific grant from funding agencies in the public, commercial, or not-for-profit sectors.

References

[1] Ye Y, Pang Z, Chen W, Ju S, Zhou C. The epidemiology and risk factors of inflammatory bowel disease. International journal of clinical and experimental medicine 2015;8:22529-42.
[2] Arnold M, Sierra MS, Laversanne M, Soerjomataram I, Jemal A, Bray F. Global patterns and trends in colorectal cancer incidence and mortality. Gut 2017;66:683-91.
[3] Kararli TT. Comparison of the gastrointestinal anatomy, physiology, and biochemistry of humans and commonly used laboratory animals. Biopharmaceutics & drug disposition 1995;16:351-80.
[4] Puértolas S, Bajador E, Puértolas JA, López E, Ibarz E, Gracia L, et al. Study of the behavior of a bell-shaped colonic self-expandable NiTi stent under peristaltic movements. Biomed Res Int 2013;2013:370582.
[5] Puértolas S, Navallas D, Herrera A, Lopez E, Millastre J, Ibarz E, et al. A methodology for the customized design of colonic stents based on a parametric model. J Mech Behav Biomed Mater 2017;71:250-61.
[6] Egorov VI, Schastlivtsev IV, Prut EV, Baranov AO, Turusov RA. Mechanical properties of the human gastrointestinal tract. J Biomech 2002;35:1417-25.
[7] Massalou D, Masson C, Foti P, Afquir S, Baque P, Berdah SV, et al. Dynamic biomechanical characterization of colon tissue according to anatomical factors. J Biomech 2016;49:3861-7.
[8] Higa M, Luo Y, Okuyama T, Shiraishi Y, Liu H, Yambe T, et al. In vivo measurements and constitutive modeling of colon tissue. Ifmbe Proc 2007;14:3186-+.
[9] Qiao Y, Pan E, Chakravarthula SS, Han F, Liang J, Gudlavalleti S. Measurement of mechanical properties of rectal wall. Journal of materials science Materials in medicine 2005;16:183-8.
[10] Ciarletta P, Dario P, Tendick F, Micera S. Hyperelastic Model of Anisotropic Fiber Reinforcements within Intestinal Walls for Applications in Medical Robotics. Int J Robot Res 2009;28:1279-88.
[11] Carniel EL, Gramigna V, Fontanella CG, Frigo A, Stefanini C, Rubini A, et al. Characterization of the anisotropic mechanical behaviour of colonic tissues: experimental activity and constitutive formulation. Exp Physiol 2014;99:759-71.
[12] Patel B, Chen H, Ahuja A, Krieger JF, Noblet J, Chambers S, et al. Constitutive modeling of the passive inflation-extension behavior of the swine colon. Journal of the Mechanical Behavior of Biomedical Materials 2018;77:176-86.
[13] Ekmektzoglou KA, Zografos GC, Kourkoulis SK, Dontas IA, Giannopoulos PK, Marinou KA, et al. Mechanical behavior of colonic anastomosis in experimental settings as a measure of wound repair and tissue integrity. World journal of gastroenterology 2006;12:5668-73.
[14] Sokolis DP, Orfanidis IK, Peroulis M. Biomechanical testing and material characterization for the rat large intestine: regional dependence of material parameters. Physiological measurement 2011;32:1969-82.
[15] Carniel EL, Rubini A, Frigo A, Natali AN. Analysis of the biomechanical behaviour of gastrointestinal regions adopting an experimental and computational approach. Computer methods and programs in biomedicine 2014;113:338-45.
[16] Shahzad M, Kamran A, Siddiqui MZ, Farhan M. Mechanical Characterization and FE Modelling of a Hyperelastic Material. Mater Res-Ibero-Am J 2015;18:918-24.

[17] Han Y, Chen JH, Wang SM. Characterisation of hyper-elastic materials by non-equibiaxial extension test based on dual- variable method. Plast Rubber Compos 2017;46:103-9.
[18] Siri S, Maier F, Santos S, Pierce DM, Feng B. The load-bearing function of the colorectal submucosa and its relevance to visceral nociception elicited by mechanical stretch. American journal of physiology Gastrointestinal and liver physiology 2019.
[19] Hidovic-Rowe D, Claridge E. Modelling and validation of spectral reflectance for the colon. Physics in medicine and biology 2005;50:1071-93.
[20] Yu J, Zeng Y, Zhao J, Liao D, Gregersen H. Quantitative analysis of collagen fiber angle in the submucosa of small intestine. Comput Biol Med 2004;34:539-50.
[21] Tong J, Cohnert T, Regitnig P, Holzapfel GA. Effects of age on the elastic properties of the intraluminal thrombus and the thrombus-covered wall in abdominal aortic aneurysms: biaxial extension behaviour and material modelling. European journal of vascular and endovascular surgery : the official journal of the European Society for Vascular Surgery 2011;42:207-19.
[22] Peña JA, Corral V, Martinez MA, Peña E. Over length quantification of the multiaxial mechanical properties of the ascending, descending and abdominal aorta using Digital Image Correlation. J Mech Behav Biomed Mater 2018;77:434-45.
[23] Moerman KM, Holt CA, Evans SL, Simms CK. Digital image correlation and finite element modelling as a method to determine mechanical properties of human soft tissue in vivo. Journal of Biomechanics 2009;42:1150-3.
[24] Grédiac M, Pierron F, Avril S, Toussaint E, Rossi P. Full-Field Measuments and Identification in Solid Mechanics. 2012.
[25] Holzapfel GA, Gasser TC, Ogden RW. A new constitutive framework for arterial wall mechanics and a comparative study of material models. J Elasticity 2000;61:1-48.
[26] Gasser TC, Ogden RW, Holzapfel GA. Hyperelastic modelling of arterial layers with distributed collagen fibre orientations. Journal of the Royal Society Interface 2006;3:15-35.
[27] Demiray H. A note on the elasticity of soft biological tissues. Journal of Biomechanics 1972;5:309-11.
[28] Baek S, Gleason RL, Rajagopal KR, Humphrey JD. Theory of small on large: Potential utility in computations of fluid-solid interactions in arteries. Computer Methods in Applied Mechanics and Engineering 2007;196:3070-8.
[29] Ferruzzi J, Vorp DA, Humphrey JD. On constitutive descriptors of the biaxial mechanical behaviour of human abdominal aorta and aneurysms. Journal of the Royal Society, Interface 2011;8:435-50.
[30] Lanir Y. Constitutive equations for fibrous connective tissues. J Biomech 1983;16:1-12.
[31] Federico S, Herzog W. Towards an analytical model of soft biological tissues. J Biomech 2008;41:3309-13.
[32] Cortes DH, Lake SP, Kadlowec JA, Soslowsky LJ, Elliott DM. Characterizing the mechanical contribution of fiber angular distribution in connective tissue: comparison of two modeling approaches. Biomechanics and modeling in mechanobiology 2010;9:651-8.
[33] Alastrué V, Sáez P, Martínez MA, Doblaré M. On the use of the Bingham statistical distribution in microsphere-based constitutive models for arterial tissue. Mech Res Commun 2010;37:700-6.
[34] Alastrué V, Martínez MA, Doblaré M, Menzel A. Anisotropic micro-sphere-based finite elasticity applied to blood vessel modelling. J Mech Phys Solids 2009;57:178-203.

[35] Bingham C. An Antipodally Symmetric Distribution on the Sphere. Ann Statist 1974;2:1201-25.
[36] Nelder JA, Mead R. A Simplex Method for Function Minimization. The Computer Journal 1965;7:308-13.
[37] Skacel P. Hyperfit software. 2019. [online] Hyperfit.wz.cz. Available at: http://hyperfit.wz.cz/ [Accessed 18 May 2019].
[38] Natali AN, Carniel EL, Gregersen H. Biomechanical behaviour of oesophageal tissues: material and structural configuration, experimental data and constitutive analysis. Med Eng Phys 2009;31:1056-62.
[39] Christensen MB, Oberg K, Wolchok JC. Tensile properties of the rectal and sigmoid colon: a comparative analysis of human and porcine tissue. SpringerPlus 2015;4:142.

Highlights

- Characterization of **mechanical hyperelastic behavior of colonic tissue.**
- **Multiaxial experimental testing** of colonic tissue by means of biaxial tests carried out in different parts along large intestine.
- **Comparative study of five hyperelastic constitutive models** for colonic tissue.
- **Fitting of elastic parameters** for the different analyzed models, accounting for the multilayered conformation of the colonic tissue.
- **Predictive capability study** of the analyzed constitutive models and determination of the most suitable for numerical simulations.